UNIVERSITY OF OKLAHOMA

GRADUATE COLLEGE

REGIONAL STRATIGRAPHY AND DIAGENETIC CHARACTERIZATION OF THE

MISSISSIPPIAN MERAMEC, OSAGE, AND SYCAMORE FORMATIONS, ANADARKO

BASIN, CENTRAL OKLAHOMA

A THESIS

SUBMITTED TO THE GRADUATE FACULTY

in partial fulfillment of the requirements for the

Degree of

MASTER OF SCIENCE

By

CORY TERRELL
Norman, Oklahoma
2019

REGIONAL STRATIGRAPHY AND DIAGENETIC CHARACTERIZATION OF THE
MISSISSIPPIAN MERAMEC, OSAGE, AND SYCAMORE FORMATIONS, ANADARKO
BASIN, CENTRAL OKLAHOMA

A THESIS APPROVED FOR THE
CONOCOPHILLIPS SCHOOL OF GEOLOGY AND GEOPHYSICS

BY

Dr. R. Douglas Elmore, Chair

Dr. Shannon Dulin

Dr. Michael Engel

TABLE OF CONTENTS

List of Figures

List of Tables

Abstract

  The principal goals of this study were to characterize the regional stratigraphy, analyze the extent of diagenetic alteration, and determine the factors controlling reservoir quality of the Meramec, Osage, and Sycamore Formations in the STACK (Sooner Trend of the Anadarko Basin in Canadian and Kingfisher counties), MERGE, and SCOOP (South Central Oklahoma Oil Province). These formations are poorly understood unconventional targets in the Anadarko Basin that overlie the Devonian to Mississippian Woodford Shale. The Mississippian Meramec, Osage, and Sycamore formations are composed of low permeability anisotropic siliciclastics and carbonate rocks with limited source potential and storage capacity.

  Regional well log correlations, petrographic analysis, core descriptions, anisotropy of magnetic susceptibility, and hand-held X-Ray fluorescence spectroscopy (HHXRF) was used to characterize the spatial and temporal relationships of the regional Mississippian stratigraphy within the study area. From this analysis, it was concluded that the lower portions of the Sycamore (Sycamore Limestone) in the SCOOP are the time equivalent of the Osage in the STACK. This work also showed that the upper portions of the Sycamore (Sycamore Shale) is the time equivalent of the STACK Meramec. These trends also point to a northern Osage source and a southern Sycamore Limestone source.

  Petrophysical analysis, HHXRF, petrographic relationships were integrated to determine that reservoir quality is lithology dependent. Marine calcite cements have occluded primary porosity within siltstones in the Meramec, Osage, and Sycamore Formations that lack detrital clay influx or bioturbation. Increased clay content prevents calcite nucleation and can preserve primary porosity as well as provide interlayer clay porosity. Porosity within the Osage and Sycamore Limestone Formations are locally enhanced as a result of meteoric diagenesis. Local

xiv

sea level fluctuations decalcified carbonates and developed enhanced secondary porosity. The Sycamore Limestone and Osage both contain fractures with hydrothermal minerals such as mega quartz and baroque dolomite that developed coeval with hydrocarbon migration.

Introduction

The Mississippi age rocks of the Anadarko Basin are an amalgamation of siliciclastic and carbonate strata that have a complex stratigraphic, structural, and diagenetic history. The Mississippian carbonates of the northern Anadarko Basin were deposited upon a stable shelf and ramp which transitioned down-dip into the deeper water siltstones and mudstones of the Osage, Meramec, and Sycamore formations. Down-dip deposition resulted in anisotropic reservoir properties, rapid facies changes, and significant hydrocarbon accumulations. These hydrocarbons are stored in primary pores, enhanced by diagenetic processes, and secondary pores.

Drilling low permeability anisotropic rocks with limited source potential has led to renewed focus on unconventional technologies by the oil and gas industry. Characterizing porosity types, fluid migration events, mechanical properties, and mineralogic variations are crucial for understanding reservoir quality. These complex drivers of reservoir quality have become increasingly important to understanding the Mississippi strata within the Anadarko Basin. This thesis will consider the spatial and temporal relationships of the Osage, Meramec, and Sycamore formations in the Anadarko Basin. To better understand the regional variations of these rocks, three distinct study areas were chosen, and subsequently, subsurface cores were located. The three areas of interest are (1) STACK (Sooner Trend of the Anadarko Basin in Canadian and Kingfisher counties), (2) MERGE, and (3) SCOOP (South Central Oklahoma Oil Province). Five whole cores, one set of sidewall core, and digital well log data from 150 public well logs within these three study areas were used in this study to characterize the stratigraphic, diagenetic, and reservoir properties of the Osage, Meramec, and Sycamore formations (Figure 1). This data set was used for the following primary goals of this study:

1

1. Define the regional stratigraphic differences and construct a depositional model for the Osage, Meramec, and Sycamore formations and determine how provenance proximity and fluctuations in accommodation space impacted stratigraphy.

2. Define the paragenesis of the relevant formations and determine if diagenetic variations are controlled by lithology (closed system) or regional fluid migration (open system).

3. Determine the extent and timing of hydrothermal alteration relative to hydrocarbon migration and fracture events.

4. Characterize the pore systems and determine regional changes.

5. Develop a XRF based facies model that can be used for reservoir characterization.

These goals will test the hypothesis that reservoir quality is dependent upon lithology for the Osage, Meramec, and Sycamore formations within the STACK, MERGE, and SCOOP. I will also test if the lower portion of the Sycamore is the time equivalent of the Osage, and the Upper Sycamore is the downdip equivalent of the Meramec. Understanding the porosity types, fluid migration events, and mineralogic variations developed through petrographic analysis, this study will allow for characterization of reservoir quality in the Osage, Meramec, and Sycamore formations within the Anadarko Basin.

Geologic Setting

The Anadarko Basin developed during Precambrian to Cambrian rifting which formed the Southern Oklahoma Aulacogen (SOA) and the Oklahoma Basin (Hoffman et al., 1974). This failed rift event emplaced igneous rocks in the Wichita and Arbuckle provinces (Figure 2)

2

and developed the linear trough for which 12 km (40,000 ft.) of Cambrian though Permian

sediment have been deposited (Figure 3) (Ham & Wilson, 1967). The basin underwent thermal

subsidence within the Southern Oklahoma Aulacogen trough through the Ordovician and

transitioned to gradual downwarping during the Silurian-Devonian (Ham et al., 1964; Garner &

Turcotte, 1984; Perry, 1989). Deposition starting in the Cambrian through the Devonian rarely

exceeded subsidence rates (Perry, 1989). Lacking significant accommodation space, the basin

was filled with shallow water carbonates, sandstones, and shales that compose the Cambrian-

Devonian strata within the early Oklahoma Basin.

During the late Devonian, subsidence increased in the northern portions of the paleo

Oklahoma Basin (Ham et al, 1964; Perry, 1989). This event allowed for the accommodation of

deeper water late Devonian-Mississippian siliciclastic, shales, and carbonate rocks (Ham et al.,

1964; Perry, 1989). Increasing subsidence during the Mississippian foreshadowed the

Pennsylvanian Ouachita Orogeny. The Ouachita Orogeny transformed the Oklahoma Basin

from an intracontinental rift basin to a foreland basin dominated by tectonic driven subsidence

and basement involved thrusting, and separated the Oklahoma Basin into the Anadarko,

Ardmore, and Arkoma basins (Ham et al., 1964; Garner & Turcotte, 1984; Perry, 1989; Mueller

et al., 2014; Domeier & Torsvik, 2014). Variable subsidence rates and increased tectonic

activity led to the stratigraphic and structural complexities of the Mississippian strata within the

Anadarko Basin.

The Mississippian Sycamore, Meramec, and Osage formations are underlain by the

Devonian-Mississippian Woodford Shale and overlain by Mississippian Caney and Chester

formations. The Woodford is the most prolific source rock in the Anadarko Basin (Johnson &

Cardott, 1992). Horizontal drilling and hydraulic stimulation has allowed for hydrocarbon

3

production directly from the Woodford source. However, as the Woodford reserves were depleted, new unconventional targets have been identified throughout the Anadarko Basin.

The Cana Woodford Field in Canadian county was the first major horizontal Woodford target in the Anadarko basin. As production declined in this field, operators began applying their advanced drilling technologies to the overlying Osage and Meramec formations. Co-developing these three formations expanded the Cana Field into the STACK (Sooner Trend Anadarko Basin Canadian and Kingfisher Counties). Further exploration of the reservoirs to the south led to increased discoveries. First, technologies learned in the Cana Field were applied to the Woodford in the SCOOP (South Central Oklahoma Oil Province) and similarly to the STACK, the overlying Mississippian Sycamore and Caney were targeted. Further exploration attempted to connect the SCOOP and STACK into the MERGE of northern Grady and southern Canadian counties.

The study area is located on the eastern margin of the Anadarko Basin and is bounded structurally to the south by the Wichita Uplift, to the east by the Nemaha Ridge, and to the north by the Anadarko Shelf. During deposition, the study area was a subtropical environment at a paleolatitude of approximately 20-30 degrees south of the palaeoequator with wind and Coriolis-driven surface currents coming from the present day northeast direction (Figure 4) (Gutshick & Sandberg, 1983; Witzke, 1990; Golonka et al., 1994; Mazzullo et al., 2009; Drummond, 2018).

Deposition of the Osage Formation occurred conformably to unconformably over the Kinderhook and Woodford shales (Figure 5) in shallow marine waters upon a distally steepened ramp near the seaward margin of the Burlington shelf (Mazzullo et al., 2009; Price, 2014). Read (1985) characterized distally steepened ramps by the presence of the downslope

gravity flows and mass transport deposits that carry shallow sediment into the basin. Osage deposition is dominated by sponges, bryozoans, crinoids, and lime mud distally from the ramp margin.

Meramecian deposition occurred distally along the Anadarko Shelf. The Meramec Formation is composed of silt to sand sized siliciclastic material with fossil debris, minor amounts of clay, and local occurrences of dolostones. Price et al. (2017) used internal mapping geometries to identify a system of prograding clinoforms with low inclinations (less than 1 degree) within the Meramec. These clinoforms contain similar facies throughout with exception of the uppermost topset (calcareous) and the lowermost bottomset (argillaceous) (Price et al., 2017). Price et al. (2017) hypothesized that the low inclination clinoforms resulted from deposition within a subaqueous delta complex (e.g. Patruno et al., 2015). Leavitt (2018) alternatively hypothesized Meramec deposition resulted from hyperpycnal flows that transported aeolian silt and detrital carbonates downdip into the basin.

The Sycamore Limestone in southern Oklahoma was first defined by Taff (1903) as a blueish to yellow wedge limestone lacking fossils with thin beds (~.3 m [~1 ft.]). Culp (1961) described the Sycamore Limestone as a finely crystalline silty limestone (up to 50% silt) with interbeds of shale and local occurrences of glauconite, muscovite, chert, and pyrite. This siliciclastic system of carbonate siltstones and mudstones transition up-dip into the Osage and Meramec Formations. Miller (2018) used log correlations to relate the Sycamore Formation that outcrops along I-35 in the north flank of the Arbuckle mountains of Southern Oklahoma to the Meramec where it is more prevalent in Blaine County. Schwatzapfel and Holdsworth (1996) used paleontological data to date the Sycamore as the Upper Meramec time equivalent. Schwartzapfel and Holdsworth (1996) identified incomplete Bouma sequences, groove and

flute clasts, contorted bedding, and a thickening/coarsening upward trend along the Sycamore outcrops in the Arbuckle mountains. Schwartzapfel and Holdsworth (1996) conclude that Sycamore deposition occurred through a mass-gravity flow process. Alternatively, Franklin (1997) concluded that the Sycamore was deposited as the result of deep surface/bottom currents. Franklin (1997) determined there was no evidence for channelized turbidity flow and the Anadarko basin lacked the needed energy to transport sediment for such long distances. However, more modern studies such as Miller (2018) have concluded that Sycamore deposition resulted from turbidity currents and gravity flows.

The Mississippian Period in the Anadarko basin represents a transitional period both structurally and stratigraphically. The Mississippian is known to be the transitional period between the greenhouse conditions of the Devonian and the icehouse period of the Pennsylvanian (Figure 6) as well as changes in ocean chemistry from calcite to aragonite seas (Read et al., 1995; Ries, 2010; Price, 2014). Globally, these fluctuations in global temperatures resulted in regressing seas. Locally, sea level changes and accommodation space were being influenced by ice volumes, tectonic activity, and sedimentation rates (Read et al., 1995). Overall, a decrease in sea level occurred during the Mississippian Period that reduced accommodation space, resulting in wedges of carbonate and siliciclastic sediment prograding into the deep sections of the Anadarko Basin (Price et al., 2017; Miller, 2018). Higher order cycles of sea level change have been attributed to the increased porosities that are found within the Mississippi Lime carbonates. Local sea level fluctuations resulted in silicification of carbonate material and leaching of calcite by meteoric fluids (Rogers, 2001). These local anomalies are likely the result of sedimentation rates or short-term climate variations that exposed the carbonate material to near surface processes.

Hydrothermal alteration has been shown to affect the mechanical properties and porosity of the Mississippi strata in Oklahoma. Roberts and Elmore (2017) found evidence of hydrothermal alteration of fractures within the underlying Woodford shale in the SCOOP study area. Roberts and Elmore (2017) hypothesized that hydrothermal fluids were expulsed and traveled up dip during the Ouachita orogenic activity that followed Mississippi deposition. Elmore et al. (2017) found evidence for a Permian remagnitization of the Mississippi Lime carbonates in north central Oklahoma and related these results to hydrothermal fluid flow events. Roberts et al. (2017) reported that hydrothermal fluids altered the Woodford Shale in the late Permian in the Ardmore Basin. Fractures and faults within the Woodford shale most likely acted as a conduit for the hydrothermal fluids. Dehcheshmehi (2016) completed a diagenetic study of the Meramec and Osage in the STACK study area and found homogenization temperatures in carbonate and quartz minerals were nearly 50°C higher than burial temperatures for the study area. Dehcheshmehi (2016) concluded that these temperatures resulted from pulses of deeper basin fluids related to Ouachita and Appalachian orogenies.

Methods

Data Collection and Sampling

Five un-oriented vertical cores and 1 set of sidewall cores were obtained to characterize the study area. Cores were chosen based on geographic distribution and accessibility. Full length plugs were extracted from the whole cores and thin sections were made from both the sidewall and whole core samples. Core availability was the greatest limit to data collection. Samples were chosen to best capture the rock types observed in core or on well logs, and features such as mineralized fractures or surface boundaries. Samples from the whole cores were trimmed to standard plug size (25 mm diameter x 22 mm height). Remnant sidewall core

7

samples were used for crushed rock analysis and mechanical property testing. Log vintage and quality varied from core to core. Core gamma ray, and other available data sources were used to depth shift the core samples to their corresponding well logs.

Core descriptions and sample collection was conducted at the Oklahoma Petroleum Information Center (OPIC) on the 5 cores that covered the Osage, Meramec, and Sycamore Formations in the study area. Core photographs and descriptions were collected to characterize rock facies and their spatial relationship on a 15 cm [~.5 ft.] scale. Facies data collected from the core was then used to determine appropriate sample locations. Doubly polished thin sections were used for the petrographic analysis (95 from the Meramec, 41 from the Osage, and 46 from the Sycamore). These 182 thin sections were impregnated with fluorescent blue dye to assist with the characterization of porosity within the samples. The thin sections were then stained with a mix of alizarin red and potassium ferricyanide. Alizarin red is commonly used for its ability to stain carbonates pink to red, and aids in the identification of minerals such as calcite and aragonite. Potassium ferricyanide was used to identify iron rich carbonates or zoned ferrous carbonates that would be stained blue (e.g. Table 1).

Petrography

Petrographic analysis was conducted on a Zeiss AxioImager.Z1m and photomicrographs were collected using the accompanied AxioVision software in reflected, ultraviolet, plane-polarized, and cross-polarized light with magnifications of up to 100x. Thin section analysis focused on determining relative diagenetic timing using cross cutting and textural relationships, characterizing pore types, understanding fracture mineralization paragenesis, and petrographic facies analysis. Geographic locations and core descriptions were not considered during petrographic analysis to prevent biasing petrographic facies

classification. Once petrographic analysis was completed, core facies descriptions and petrographic facies descriptions were compared to validate observations in both hand sample and microscopic scales.

Scanning electron microscopy (SEM) was critical for determining textural and cross cutting relations as well as characterizing mineral phases that were unidentifiable in transmitted or reflected light. The FEI Quantam 250 SEM with back scattered electron imaging (BSE) and secondary electron imaging (SE) was used in conjunction with the Bruker XFlash x-ray detector (EDX) to accurately determine paragenesis, mineralogy, and identify micro pore systems.

Hand-Held X-Ray Fluorescence (HHXRF)

Hand-held x-ray florescence (HHXRF) analysis was conducted to quantitatively characterize the elemental, diagenetic, and facies variations of the Mississippi strata within the study area. A total of 109 plugs were analyzed using a Bruker Traver III HH-XRF Spectrometer. Major elements (Si, Al, Fe, Mg, Ca, K, Ti) were scanned under vacuum at 15kV accelerating voltage for 90 seconds. Trace elements (Sr, Pb, Th, V, Ni, Cu, Zr, Nb) were analyzed under normal conditions at a 40-kV accelerating voltage for 60 seconds. Raw HHXRF data was calibrated using the fine-grained sedimentary rock methodology from Rowe et al. (2012).

HHXRF data is reported in PPM and can be converted to weight percent (Wt.%). Using these values, the elemental data was used for inferring mineralogy, brittleness, total organic carbon (TOC), redox conditions, provenance, and depositional environments. Combining these factors, chemofacies were developed to characterize facies developed through core and thin section analysis. To compare the chemofacies and lithofacies directly, a synthetic chemo-

gamma was produced to tie the core gamma and logged gamma data points. The synthetic

chemo-gamma was calculated using a spectral gamma ray technique, where

$GR_{Chemo}=4*(U_{ppm})+8*(Th_{ppm})+16*(K_{Wt\%})$ (Asquith et al., 2004).

K, Al, and Th were used as proxies for clay concentrations, Si was used for relative

quartz concentrations, Ca and Sr were used as carbonate proxies, Mo and V were used as

proxies for anoxic bottom water conditions, and Ti, Zr, and a ratio of Ti to Nb (Ti/Nb) were

used for provenance indicators (Table 2) (Sageman and Lyons, 2003; Tribovillard et al., 2006;

Turner et al., 2016, Duarte, 2018; Heij, 2018).

Chemofacies were developed using the unsupervised K-means clustering technique

(Kanungo et al., 2002). This clustering method allowed for clustering of like chemical

components which were then assigned to a chemofacies. K-means clustering and principal

component analysis was completed in RStudio 1.1.463. The data was reduced to represent only

one chemical proxy for each mineralogical/environmental component. The variables include Al

(clay), Si (quartz), Ca (carbonate), Zr (continental source proxy), and V (anoxic bottom water

proxy). These variables were transformed to standardize the data such that each variable had a

mean of zero and standard deviation of one. The correct number of clusters (K) was determined

through the elbow method. This method plots the summed distance of the data for successively

increasing clusters. K is determined at the inflection point where the increase in clusters no

longer affects the variance in the data. These chemofacies were then compared to lithofacies

data collected in the whole core and petrographic analysis.

Anisotropy of Magnetic Susceptibility (AMS)

AMS data was collected on 69 plug samples that were trimmed to standard plug size (25

mm diameter X 22 mm height) from the 5 whole cores that were analyzed in the study area.

This data was collected using a KLY-4S Kappabridge magnetic suceptimeter and analyzed using the Anisoft 5.1.01 software. AMS data is collected by measuring the orientation dependent heterogeneities of induced magnetization when a magnetic field is applied to a rock sample containing magnetic minerals (Hrouda, 2002; Hrouda et al., 2006; Dubey, 2014). Sedimentary mineral grains preferentially orientate when exposed to an applied magnetic field, which are then preserved during deposition (Dubey, 2014). Petrofabrics in this study were measured using low field magnetic susceptibility. Low field magnetic susceptibility (K) is the ratio of the strength of the induced magnetization (M, dipole moment per unit volume or J, dipole moment per unit mass) to the strength of the applied low field magnetic field (H) (Tarling & Hrouda, 1993; Dubey, 2014; Heij, 2018).

$$K=M/H$$

The anisotropic magnetic susceptibility (K) of the rock is then represented as a second order symmetric tensor and can be plotted with three principle axes on an ellipsoid. The axes are composed of the maximum magnetic susceptibility (K1), the intermediate magnetic susceptibility (K2), and the minimum magnetic susceptibility (K3), where K1>K2>K3. The degree of anisotropy (Pj) is defined as the difference of the maximum and minimum magnetic susceptibility (K1 and K3) relative to the average susceptibility (Kmean), where Kmean=(K1+K2+K3)/3 (Dubrey, 2014).

$$Pj= K1-K3/Kmean$$

The shape parameter (T) is defined as T=(2*ln(K2)-ln(K1)-ln(K3))/(ln(K1)-ln(K3)) (Jelinek, 1981). Plotting this data on a Jelinek Shape Plot with Pj along the horizontal axis, and T along the vertical axis (-1<T<1) allows for determining if a sample has a prolate or oblate petrofabric (e.g. Figure 7) (Jelinek, 1981; Dubrey, 2014).

Mapping

A key aspect of this study was to understand the regional stratigraphic differences and to construct a depositional model for the Osage, Meramec, and Sycamore Formations. The use of log correlations to develop both stratigraphic and structural cross sections as well as structure and isochore maps supplemented with petrographic analysis was crucial to this understanding. Log correlations require extensive regional understanding to be consistent over large geographic areas. The Mississippi rocks in the Anadarko basin require special attention due to rapid facies changes and structural anomalies. Therefore, over 10,000 well logs in the Anadarko Basin acquired through IHS Enerdeq were analyzed to develop a regionally consist stratigraphic framework (Figure 5). Many of the logs from this data are not in the study area, however, understanding the regional geology is crucial for accurately analyzing local geologic phenomena.

Once a regional stratigraphic framework was constructed, intraformational Woodford, Osage, Meramec, and Sycamore picks that focused on interpreted maximum flooding surfaces were developed locally within the Mississippi interval to better correlate stratigraphic changes throughout the study area. A regional cross section was developed that spanned north to south from the STACK in Blaine County to the SCOOP in northern Stephens County. A subsea structure map was developed on the regionally consistent underlying Woodford top. Isochore maps were constructed on the formations of interest to show the thickness of each unit in the subsurface. Digital logs were obtained through digitization of raster images and 150 raster images were digitized. Wells for digitization were selected based on geographic locations and log quality. Wells that had a GR curve in the interval were selected, with many of the wells having a triple combo data set (GR, ResD, DPHI, NPHI).

Vshale and total porosity models were developed based on available core data to aid in the understanding of regional stratigraphic variability both in cross section and in mapping. Electro facies were not developed in this study. However, the data collected could be used to construct a petrophysical workflow for better predicting regional facies changes. The Vshale model was constructed with a focus on the GR log which was the most common data set in the study area. The GR based Vshale model was normalized to the available X-Ray Diffraction (XRD) data obtained through core analysis. A similar model could be applied locally using the less common DPHI and NPHI curves and possibly yield a more precise match to clay volumes reported in XRD. The GR curves used in this model were normalized locally based on standard field specific high and low average GR values. Total porosity (PHIA) was calculated using the NPHI and DPHI curves, where PHIA = $\sqrt{(NPHI^2 + DPHI^2)}$.

Results and Interpretations

Lithofacies

Whole core and thin section analysis focused on characterizing lithofacies and diagenetic alteration in the Osage, Meramec, and Sycamore Formations. First, rock samples were divided into carbonate and non-carbonate rock types based on visual inspection. From this analysis, two carbonate facies and six non-carbonate facies were observed in the three formations within the study area. These facies are: 1) sandy fossiliferous packstone, 2) calcitic siltstone, 3) argillaceous siltstone, 4) bioturbated siltstone, 5) silty mudstone, 6) glauconitic siltstone, 7) argillaceous spiculite, 8) argillaceous mudstone (Figure 8).

Sandy fossiliferous packstone (Figure 9): The sandy fossiliferous packstone is a carbonate facies composed of detrital sub-angular fine quartz sand grains (~40%), fragments of crinoids, brachiopods, bryozoans (~30%), peloids (~20%), and minor amounts of clays and

alkali feldspars (~10%). Wavy bedding and cross-stratification was observed in the core

samples containing this facies. The sandy fossiliferous packstone is the main facies in the

Osage Formation in the STACK study area with local occurrences in the Meramec sections of

the MERGE. Calcite and chalcedony cement is pervasive and occludes primary porosity that

was preserved during deposition and prior to compaction between mineral grains. Minor

amounts of porosity can be observed within skeletal grains and peloids (Figure 10-A).

Calcitic Siltstone (Figure 11): The calcitic siltstone is a carbonate facies with fine to

coarse sub-rounded detrital silt grains (~30%), detrital carbonate skeletal fragments and

carbonate peloids (~60%), and minor amounts of detrital feldspar (~5%), and clay minerals

(~5%). The calcitic siltstone is found throughout the study area within the Osage, Meramec,

and Sycamore Formations. The calcitic siltstone is massive and highly fractured with both

induced and calcite mineralized fractures. Locally, the calcitic siltstone has minor bioturbation,

planar laminations, wavy bedding, and is often interbedded with the more clay dominant

bioturbated siltstone facies. Overall, the calcitic siltstone is composed of finer grained detritus

and is lacking the abundance of fossil fragments that is found in the sandy fossiliferous

packstone. Pores are present in peloids and locally where feldspars have been dissolved after

the initial calcite cement formed (Figure 10-B).

Argillaceous Siltstone (Figure 12): The argillaceous siltstone is composed of detrital

clay (~50%), detrital silt (~30%), detrital plagioclase and alkali feldspars (~10%), and

carbonate material in the form of broken skeletal fragments and peloids (~10%). The

argillaceous siltstone is found primarily in the Meramec and Sycamore Formations within the

study area. In core, the argillaceous siltstone is dark grey with planar bedding, and locally has a

scour contact with overlying calcitic siltstone beds. The argillaceous siltstone has minor

fracturing in thin section and core samples that terminate in intervals with increased clay content and reduced silt and carbonate. Interbeds composed of highly brittle calcitic siltstones and more ductile argillaceous siltstones results in a complex mechanical stratigraphy in the Meramecian and Osagean rocks. Overall, the argillaceous siltstone has a reduced carbonate cement compared to the sandy fossiliferous packstone and calcitic siltstone with clay filling intergranular pores. The argillaceous siltstone has a much higher total porosity (~4-10%) when compared to the other carbonate dominated facies. These higher porosity values are related to porosity within clay grains that may not be effectively connected (Figure 10-C) and as a result of detrital silt clay coats that preserve intergranular porosity.

Bioturbated Siltstone (Figure 13): The bioturbated siltstone is composed of clay (~50%), silt (~30%), and carbonate minerals (~20%) as calcite and dolomite cements. The bioturbated siltstone occurs within the Osage, Meramec, and Sycamore Formations. This rock type is also relatively heterogeneous with ductile clay burrows and brittle calcite cemented packages disseminated throughout system. This siltstone is heavily bioturbated and massively bedded with minor planar laminae. Core samples from the bioturbated siltstone are dark grey to black and are interbedded with the argillaceous and calcitic siltstone lithofacies. The intervals with heavy bioturbation are composed of planolites burrows which are actively back filled with organic and clay material (Knaust, 2017). These clay rich burrows prevent calcite cement nucleation around silt grains and clay material, thus, preserving primary intergranular porosity.

Silty Mudstone (Figure 14): Silty mudstones were mostly found in the Meramec and Sycamore Formations with minor occurrences in the lower Osage. The mudstone is dark grey to black in core, with considerable amounts of clay (~60%), silt (~30%), and dolomite (~5%), and micas (~5%). Local occurrences of broken shell fragments and spicules are present. Silty

mudstones commonly overly the argillaceous and bioturbated siltstones and could result from transgressive depositional processes that produce a more distal rock facies.

Glauconitic Siltstone (Figure 15): The glauconitic siltstone occurs most notably at the Devonian and Mississippian transition between the Woodford Shale and Mississippian siliciclastic and carbonate rocks. Cores from the STACK, MERGE, and SCOOP portions of the study area contain this thin transition zone. This thinly bedded (7.62 cm [~3 in]) glauconitic siltstone facies designates a transition to a regressive cycle with increased carbonate influx. The glauconitic siltstone is composed of glauconite pellets (~70%), silt (~20%), micas (~5%), and calcite (~5%). Mazzullo (2014) hypothesized that this transitional glauconite could be the Kinderhookian Bachelor Sandstone Formation. The Glauconitic siltstone is overlain by most commonly a fine grained silty mudstone. Glauconite is much denser and is more conductive than the overlying siltstones and underlying shales and is easily distinguishable on log correlations throughout the study area.

Argillaceous spiculite (Figure 8): The argillaceous spiculite facies is composed of quartz rich spicules (~60%) with clay (~40%). Argillaceous spiculites were found only in the lower portions of the Osage and Sycamore Formations. Clay minerals fill intergranular pores between spicules.

Argillaceous mudstone (Figure 8): Clay (~90%), minor amounts of silt (~5%), and dolomite (~5%) make up the argillaceous mudstone facies. The argillaceous mudstone is planar laminated and occurs in the upper portion of the Sycamore and lower portion of the Osage Formation. Underlying the argillaceous mudstone is most commonly the silty mudstone.

Osage Lithofacies and Paragenesis

The Humble Lloyd L Hawkins #1 core (2,354 to 2,444 m [7,725 to 8,020 ft.] MD) was

taken over the lower sections of the Meramec (2,354 to 2,404 m [7,725 to 7,890 ft.] MD) and Osage (2,404 to 2,441 m [7,890 to 8,010 ft.] MD) formations in the STACK portion of the study area (Figure 16). Eight facies were characterized in the Osage Formation from forty-one thin sections and core analysis. These facies are: 1) sandy fossiliferous packstone, 2) calcitic siltstone, 3) argillaceous siltstone, 4) bioturbated siltstone, 5) silty mudstone, 6) glauconitic siltstone, 7) argillaceous spiculite, and 8) argillaceous mudstone (Figure 8).

Diagenesis within the Osage Formation facies occurs within the matrix and allochem grains (Figure 17). Minor amounts of sigmoidal veins, interpreted as pre-compactional, occur within the Osage (Figure 18-A). These pre-compactional veins are dominantly mineralized with calcite cement. Mollusk fragments underwent solution and reprecipitation processes that converted their aragonite composition to calcite. Skeletal fragments within the carbonate facies are heavily micritized. Micritization of these bryozoan and echinoderms allochems is interpreted to occur early in near surface conditions (Bathurst, 1966). Bioturbation in the form of Planolites burrows most likely occurred coeval with the micritization. These burrows are clay rich and prevented calcite nucleation around allochem fragments and detrital grains. Quartz overgrowths occur on the abundant silt and sand sized quartz grains throughout the facies in the formation. Calcite isopachous cement that is interpreted to be syndepositional has been locally decalcified and replaced by chert due to meteoric fluid alteration as a result of a decrease in local sea level and subaerial exposure. This cross cutting relationship dates the relative formation of chert to be later than the isopachous calcite cement. Minor amounts of unaltered dolomite (Figure 18-B) and dedolomite (Figure 18-C) replaces the chert cement which requires the dolomitization and dedolomitization to occur prior to chertificiation. Chert and spicule dissolution (Figure 18-D) enhanced secondary porosity within the Osage allowing

17

for hydrocarbon migration into the reservoir. Mega quartz and baroque dolomite can be seen

filling fractures in the Osage Formation (Figure 18-E). Late fracturing occurs coeval with

hydrothermal alteration and fractures are occluded by chert (Figure 18-F). The earlier chert and

spicule dissolution is a potential source for this late silica cementation.

Meramec Lithofacies and Paragenesis

Four cores were analyzed that covered portions of the Meramec Formation in the

STACK and MERGE portions of the study area. The Humble Lloyd L Hawkins #1 core was

taken over the lower sections of the Meramec in the STACK (2,354 to 2,404 m [7,725 to 7,890

ft.] MD) (Figure 16). The Schaeffer #1-23 was taken over the upper Meramec in the STACK

(2,941 to 3,014 m [9,650 to 9,890 ft.] MD) (Figure 19). The Skaggs Ranch #1-9 was taken over

the lower portions of the Meramec in the MERGE (2,965 to 2,972 m [9,730 to 9,752 ft.] MD)

(Figure 20). The Payne #1 was taken in the upper Meramec in the Merge (2,711 to 2,733 m

[8,895 to 8,967 ft.] (MD) (Figure 21). Six facies were characterized in the Meramec based on

core analysis and ninety-five thin section descriptions. These facies are: 1) sandy fossiliferous

packstone, 2) calcitic siltstone, 3) argillaceous siltstone, 4) bioturbated siltstone, 5) silty

mudstone, and 6) glauconitic siltstone (Figure 8).

Meramec diagenesis is dominated by near surface subaqueous processes that produced

authigenic phases within the matrix followed by fracturing and hydrocarbon migration (Figure

22). Fossil fragments show micritization that occurred following depositional processes. Early

framboidal pyrite that results from sulfate reduction (Folk, 2005) is cross-cutting the micritized

fossil fragments. Planolites burrows are enriched in clay and sand sized grains of quartz and

feldspar. Outside of these burrows, silt grains and peloids are cemented with a pre-

compactional calcite cement (Figure 23-A). This cement formed within the intergranular

porosity that was preserved prior to compaction. After near surface phases were produced, the

Meramec Formation began to undergo compaction and chemical dissolution producing

stylolites (Figure 23-B). The sand and silt sized quartz grains developed quartz overgrowths

(Figure 23-C). Fractures cross cut these chemical compaction features and were mineralized

with calcite cement (Figure 23-D). Following the precipitation of calcite cement in these

fractures, feldspars began to dissolve and produced clay minerals and intragranular porosity

(Figure 10-C and Figure 23-E). This porosity within clay grains and feldspars is lined with

bitumen. Intragranular feldspar pores would have been occluded by calcite cement preventing

the bitumen lining. However, organic acids related to hydrocarbon migration could have

dissolved calcite that has replaced feldspars and allowed for the bitumen to fill the pores

(Figure 23-F).

Sycamore Lithofacies and Paragenesis

One core and one set of sidewall plugs were analyzed from the Sycamore Formation in

the SCOOP portion of the study area. The Chitwood Harris #1 core was recovered over the

lower portion of the Sycamore in the SCOOP (4,567 to 4,541 m [14,809 to 14,899 ft.] MD)

(Figure 24). The sidewall plugs were acquired in well "X" over the entire Sycamore Formation

(4,178 to 4,287 m [13,710 to 14,065] MD) (Figure 25). The sidewall plugs were sampled to

represent well log derived rock types with an average sample interval of 4.5 m (15 ft.). Seven

facies were observed from analysis of the core data and 46 thin sections. These facies are: 2)

calcitic siltstone, 3) argillaceous siltstone, 4) bioturbated siltstone, 5) silty mudstone, 6)

glauconitic siltstone, 7) argillaceous spiculite, and 8) argillaceous mudstone (Figure 8). Facies

2) calcitic siltstone, 3) argillaceous siltstone, 5) silty mudstone, and 7) argillaceous spiculite

were observed in the Sycamore Limestone member. Facies 2) calcitic siltstone, 3) argillaceous

siltstone, 4) bioturbated siltstone, 5) silty mudstone, and 8) argillaceous mudstone were observed in the Sycamore Shale member.

Diagenesis within the Sycamore Formation is controlled first by near surface cement precipitation and then by compaction and fracturing (Figure 26). Early marine calcite cements surround fossil fragments, peloids, and silt sized grains within the Sycamore. Early pre-compactional veining is also mineralized primarily by calcite (Figure 27-A). Early framboidal resulting from sulfate reduction (Folk, 2005) is found in the Sycamore (Figure 27-B). Brachiopods composed of calcite are locally partially dissolved and could be a source for the calcite cements found in the Sycamore. Mechanical compaction aided in dissolution of the early carbonate cements enriching the stylolite features in quartz silt grains, clay minerals, and framboidal pyrite that were more resistant to dissolution than the carbonate minerals. Fracturing within the Sycamore is highly complex with multiple cross cutting fracture patterns and are filled with quartz, mega quartz, dolomite, dedolomite, calcite, and bitumen (Figure 27-C and Figure 27-D). Some fractures are lined with baroque dolomite that has been dissolved and replaced by silica cements. Chert locally occludes porosity within calcite that has been dissolved (Figure 27-D). Quartz overgrowths on silt grains occur during the later stages of diagenesis with no observed fractures cross cutting these features.

HHXRF Elemental Analysis

Elemental analysis was used to first understand the chemical composition of lithofacies interpreted from thin section analysis, and then to construct chemofacies for the Osage, Meramec, and Sycamore Formations. The correlation matrix in Table 3 shows the correlation between elements that are interpreted to be proxies for environmental conditions during deposition or mineral assemblages (Table 2). Lithofacies were ranked visually by increasing

20

clay content and decreasing carbonate content and compared to the mineral assembles to verify correct facies interpretations. Table 3 highlights the elements and ratios that have a strong positive correlation greater than .5 (Al vs. K, Al vs. Ti, Al vs. Th, Al vs. Mo, Al vs. Ti/Nb, Si vs. K, Si vs. Th, Si vs. Mo, K vs. Ti, K vs. Th, K vs. Mo, K vs. Ti/Nb, Ca vs. Sr, Ti vs. Th, V vs. Mo, and Th vs. Mo) and the elements and ratios that have a strong negative correlation that is less than -.5 (Al vs. Ca, Al vs. Sr, Si vs. Ca, Si vs. Sr, K vs. Ca, K vs. Sr, K vs. Si/Al, Ca vs. Ti, Ca vs. Th, Ca vs. Mo, Ti vs. Sr, Ti vs. Si/Al, Th vs. Sr, Th vs. Si/Al, Sr vs. Mo, and Si/Al vs. Ti/Nb). The elements and ratios between .5 and -.5 are interpreted to have no significant correlation.

The correlation matrix highlights the mineral and environmental proxies that are correlatable. The strongest positive correlations implying that the elements occur together are between elements that are clay mineral proxies (Al vs. K, Al vs. Th, K vs. Th), continental proxies (Al vs. Ti), and carbonate proxies (Ca vs. Sr).The strong negative correlations, implying these elements co-occur less frequently, are between clay mineral proxies and carbonate proxies (K vs. Ca, K vs. Sr, Al vs. Ca, Al vs. Sr, Th vs. Ca, and Th vs. Sr) implying an inverse relationship between clay content and carbonate content.

Plotting the Th vs. K data collected from the HHXRF allows for an estimate of clay types (Schlumberger, 1991). The Th vs. K ratio for the data collected plots primarily in the illite and mixed layer clay region of the graph (Figure 28-A). The Th vs. K relationship is the strongest of the clay mineral proxies. The Th vs. K correlation is linear and not dependent upon lithofacies. However, carbonate facies plot on the lower end of the chart with more clay rich facies gradationally plotting on the higher end of the chart. This relationship is inversely observed when comparing the Ca vs. Sr (Figure 28-B). The more carbonate rich facies plot on

21

the higher end of the Ca vs. Sr plot, while the more clay rich facies plot on the lower end of the

Ca vs. Sr plot. Comparable to the Th vs. K relationship, the slope of Ca vs. Sr is linear and

shows no facies dependency. Plotting the Ti/Nb ratio vs. Zr shows a linear trend that plots

below 500 implying a quartzofeldspathic source (Figure 29) (Bonjour & Dabard, 1991; Heij,

2018). The rock samples collected from the Sycamore Shale in the SCOOP show an increased

Ti/Nb ratio and a decreased Zr abundance. Therefore, it can be interpreted that these samples

came from a more mafic source that is different than the time equivalent Meramec in the

MERGE and STACK.

HHXRF Chemofacies

Chemofacies were defined to group rock samples that showed similar elemental

components. K means clustering was used for developing the chemofacies and the appropriate

number of clusters were determined using the elbow method (Hartigan and Wong, 1979). As

defined in the methods section, variables chosen were considered to not be co-occurring (e.g.

Ca vs. Sr). The appropriate number of chemofacies determined from the inflection point of the

Elbow Plot was four (Figure 30). The four chemofacies are plotted in Figure 30 to analyze the

amount of calcium within each chemofacies (Figure 31-A). Of these chemofacies, Chemofacies

1 and 2 have average calcium concentrations greater than 15,000 ppm. Chemofacies 1 is

composed of the highest amount of calcium of the four chemofacies with average calcium

concentrations over 28,000 ppm. Chemofacies 3 and 4 contain lower average calcium

concentrations of 12,000 ppm and 10,000 ppm, respectively.

The four chemofacies are plotted in Figure 31-B to compare the chemofacies to

aluminum concentration which is interpreted to be a clay proxy. Chemofacies 4 contains the

highest average concentration of aluminum at over 44,000 ppm. Chemofacies 4 aluminum

values range from 20,000 to 70,000 ppm. Chemofacies 3 has an average aluminum abundance

of 27,000 ppm. Chemofacies 2 contains an average of 11,000 ppm of aluminum. Chemofacies 1

has an average of 6,000 ppm of aluminum. Chemofacies 1 and 2 contain the highest amount of

the carbonate proxy calcium and the lowest amount of the clay proxy aluminum. Chemofacies 3

and 4 contain the highest amount of aluminum and the lowest amount of calcium.

Comparing these chemofacies to the principal components that compose 80% of the

data variability and overlaying the eigenvector for each variable from the clustering shows that

chemofacies 1 is the highest Ca dependent facies (Figure 32). This correlation with Ca is a

result of the carbonate that occurs within the allochem grains and carbonate cements.

Chemofacies 2 is related to an increase in Zr. Chemofacies 2 contains high Ca concentrations

and high Zr concentrations. This implies that chemofacies 2 was sourced from a continental

detritus and contains carbonate in the form of carbonate cements and/or carbonate allochems.

Chemofacies 3 has a minor carbonate dependency, but is primarily dependent upon Si and Al.

Chemofacies 3 is interpreted to have increase clay and quartz content related to silt or from

silica cements with minor amounts of carbonate allochems or carbonate cements. Chemofacies

4 has the highest dependency of Si, Al, and V (Figure 32). These three elements are proxies for

quartz, clay, and organics. Therefore, chemofacies 4 has the highest abundance of organics,

clay, and silt.

Anisotropy of Magnetic Susceptibility (AMS)

Forty-three of the sixty-nine samples that underwent AMS testing show an oblate

petrofabric. This fabric is primarily related to compaction of clay minerals following

deposition, and has been correlated to increased adsorption capacity of organic matter to the

clay surface (Parés, 2015; Heij, 2018). The remaining twenty-six of the sixty-nine samples

show a prolate texture that is dominated by framework grains and commonly results from

ferroan dolomite (Heij, 2018). Chemofacies 4 has the highest occurrence of oblate petrofabrics

(T>0) (Figure 33). Chemofacies 4 is interpreted to by the most clay rich chemofacies and shows

increasing anisotropy with an increase in shape factor (Figure 33 and 34). Chemofacies 3 has

the widest range of both oblate and prolate petrofabrics which implies varying concentrations of

Fe-bearing minerals, varying rock textures, and/or heavy diagenetic alteration (Figure 33 and

34). Chemofacies 1 has a low average degree of anisotropy (<1.02), but contains both oblate

and prolate petrofabrics (Figure 33 & 34). Chemofacies 1 has the highest carbonate

concentration and varying amounts of ferroan dolomite or calcite could explain the oblate to

prolate texture.

AMS data was grouped based on lithofacies descriptions. The calcitic siltstone and

sandy fossiliferous packstone have both oblate and prolate textures with the calcitic siltstone

being primarily oblate (T>0) (Figure 35). The calcitic siltstone shows increasing anisotropy (P)

with increasing shape factor (T) (Figure 36). Increased fracturing was observed in the carbonate

dominated facies in core and thin section. The prolate texture could be related to natural

fracturing that affected the most brittle facies irregularly throughout the study area. The clay

dominated facies have a dominantly oblate texture related to compaction of the clay minerals

(Figure 35 and 36). However, the argillaceous spiculite contains a dominant prolate texture

(T<0). This prolate texture could be related to the elongate physical character of the spicules

which underwent little mechanical compaction. The sandy fossiliferous packstone and silty

mudstone have a minor prolate AMS texture. The sandy fossiliferous packstone is dominated

by carbonate cements with varying Fe concentrations. Schmidt et al. (2007) showed that Fe-

bearing carbonates such as calcite, dolomite, and magnesite could develop oblate to prolate

petrofabrics because of these higher Fe concentrations. Minor amounts of ferroan dolomite were observed in the silty mudstone facies, which could also account for its prolate texture.

Mapping

The mapping portion of this project correlated the Osage, Meramec, Sycamore, Caney, Kinderhook, and Woodford Formations of the STACK, MERGE, and SCOOP. Correlating the Osage Formation of the STACK into the Merge, prograding clinoforms (Figure 37) thin to the south before eventually becoming thin clay-rich beds. The paleo Woodford structure most likely controlled Osage, Meramec and Sycamore deposition throughout the Anadarko basin (Figure 38). The current Woodford structure correlates to stratigraphic and facies changes as well as erosional unconformities within the Mississippian system. The deepest portion of the basin was to the southwest and the Mississippi system thins and becomes increasingly clay rich to the northeast.

The detritus rich clinoforms of the Osage can be correlated to the Sycamore Limestone in the SCOOP (Figure 37). The clinoforms of the Osage and Sycamore Limestone are bounded by an uppermost topset composed of a calcitic siltstone and the lowermost bottomset composed of an argillaceous mudstone. In the SCOOP, the clinoforms increase in thickness to the south and are bounded to the north by rapid facies change like what seen in the northern portions of the MERGE (Figure 39). This facies change is related to a thickening of the underlying Kinderhook Formation and that resulted from changing depositional processes from shelf to slope settings. However, the correlative Sycamore Limestone and Osage clinoforms migrate towards each other and thin in the same direction (Figure 37 and Figure 39). Therefore, it can be hypothesized that these progradational wedges resulted from reduced accommodation and sediment influx coming from multiple directions with the basin center occurring near the clay

25

rich portions of the MERGE. These clinoforms are conformably overlain by the Meramecian aged rocks through the main portions of study area. Close to the Nemaha Ridge on the western portions of the study area, erosion of the Osage and Sycamore limestone results in thinning of the Osagean and Meramecian rocks (Figure 39).

The Meramec was correlated to the Sycamore Shale member that overlies the Sycamore limestone (Figure 37). Moving south out of the STACK, the Meramec increases in clay content and shows a decrease in bed thickness of the calcareous and silt rich beds. Clinoforms like what is observed in the Osage can be seen thinning to the south out of the main Meramec depositional fairway (Figure 37 and Figure 40). Outside of this main depositional fairway, the Sycamore Shale and Meramec are composed of sediment-starved lime mud and fine silt seen in the Meramec facies descriptions from the Skaggs Ranch #1-9 and Payne #1 core descriptions and thin sections. The Meramec clinoforms are composed of fining upward sequences with bottomsets composed of a silt fossil hash and the topsets composed of argillaceous mudstones. This relationship can be seen in Figure 37 and in more detail in the core descriptions from Figure 16, 19, 21, and 24 from the Chitwood Harris #1, Payne #1, Humble Hawkins #1, and the Schaeffer #1 well logs. The top of the Meramec and Sycamore Shale is correlated as a sharp decrease in resistivity and an accompanied increase in NPHI related to an increase in clay content of the conformably overlain Chesterian Formations (Caney in the SCOOP and Manning in the STACK) (Figure 3).

Discussion

Stratigraphy

The Osage Formation in the STACK resulted from deposition on the distal portion of a steepened ramp and is composed of gravity flows and mass transport deposits that prograde into

26

the Anadarko Basin from the north (Figure 37) (Mazzullo et al., 2009; Price, 2014). These flows resulted in massive indurated beds composed of silt, peloids, and fossil fragments. As these flow units became sediment starved distally into what is now the MERGE, the carbonate material decreased and silt and clay increased. This resulted in the deposition of thin clay beds and fine detritus.

The top of the Osage is correlated in well logs at the inflection point of a resistivity decrease, and an increase in GR as well as NPHI and DPHI (Figure 3). This is related to an overall increase in clay content of the overlying Meramec depositional system. This log response is also observed in the southern Sycamore Formation and leads to the correlation of the Osage to the Sycamore Limestone (Figure 3).

The Sycamore Limestone of the SCOOP consists of well indurated massive calcareous beds composed of coarse silt, peloids, and fossil fragments. Progradational wedges of sediment are observed migrating north out of the SCOOP into the MERGE and become increasing clay rich before pinching out. These wedges resulted from a decrease in proximal accommodation space that forced sediment into the deeper portions of the basin on a distal ramp complex. Using core descriptions and log correlations from this study as well as interpretations from Schwartzapfel and Holdsworth (1996) and Miller (2018), it can be concluded the Sycamore Limestone resulted from gravity flows and turbidity currents that developed incomplete Bouma sequences, groove and flute clasts, and contorted bedding. The Osage and Sycamore Limestone are time equivalent formations and were derived from a northern (Osage) and southern (Sycamore Limestone) sediment source (Figure 37).

The Meramec Formation in the STACK and MERGE resulted from different depositional processes compared to the Osage. The Meramec is composed of increasing clay-rich argillaceous

27

siltstones and silty mudstone lithofacies that were deposited near storm wave base with coarser

calcitic siltstone facies that are interpreted to represent deposition near fair weather wave base.

The Meramec is made of low angle prograding clinoforms that prograded north to south upon the

low angle Anadarko Ramp (<1°) (Price et al., 2017; Miller, 2018). These clinoforms show signs

of incomplete Bouma sequences and are composed of stacked harmonic parasequences lobes

with an overall coarsening upward sequence (Price et al., 2017; Miller, 2018).

The top of the Meramec is marked by a sharp decrease in resistivity and an overall

increase in GR and NPHI (Figure 3). These petrophysical property changes result from an

increase in abundance of conductive clays within the overlying Chesterian Caney and Manning

shale Formations. This log response is observed in the correlative Sycamore Shale that overlies

the Sycamore Limestone within the SCOOP (Figure 3)

The Sycamore shale is more clay-rich compared to the Meramec. The deposition of the

Sycamore Shale within the SCOOP likely records a shift to a deeper water basinal setting away

from the main Meramec depositional fairway in the STACK. The chemostratigraphic properties

of the Sycamore Shale also show an overall increase in Mo and V which is interpreted to record

an overall increase in bottom water anoxia and euxinic conditions (Turner et al., 2016; Duarte,

2018). Subsidence following Sycamore Limestone deposition resulted in an increase in

accommodation space that allowed for the deeper water Sycamore Shale sediments to

accumulate in the SCOOP.

Osage and Sycamore Limestone Diagenesis

The main diagenetic features that impact porosity of the Osage and Sycamore

Limestone Formations occur prior to and during compaction. The relative paragenetic timing is

characterized by marine cements and compaction features such as stylolites. These formations

have pre-compactional veins mineralized with calcite cement and skeletal fragments that are heavily micritized. Silt grains and peloids are heavily cemented with calcite and show a floating texture implying cementation occurred prior to compaction. Calcite cement is partially to totally replaced within the Osage by chert. This decalcification process that results in microporous tripolitic chert is observed throughout the Mississippi carbonates of northern Oklahoma and southern Kansas (Rogers, 2001; Mazzullo et al., 2009; Price et al., 2014; Manger, 2014; Hardwick, 2018). The formation of chert within the Osage and Sycamore Limestone results from subaerial exposure related to high order sea level cyclicity and decreased accommodation space, which resulted in the carbonate rocks being decalcified by meteoric fluids prior to compaction (Figure 18-B and Figure 18-C) (Rogers, 2001; Hardwick, 2018).

Following the near surface diagenetic alterations, the Osage and Sycamore Limestone Formations underwent burial and compaction that developed stylolites and mineralized fractures. These fractures contain authigenic phases that are related to hydrothermal activity such as mega quartz, calcite, and baroque dolomite. These phases are similar to the reported hydrothermal alteration of the Mississippi Limestone of Northern Oklahoma and Southern Kansas and are possibly related to MVT mineralization during the Pennsylvanian or Early Permian (Manger, 2014; Goldstein & King, 2015; Elmore et al., 2015).

Meramec and Sycamore Shale Diagenesis

Marine calcite cement is the most pervasive authigenic phase in the Meramec Formation. In the Sycamore Shale, skeletal fragments are heavily micritized and transitional facies between the calcitic siltstones and argillaceous siltstones are highly altered by bioturbation. Some skeletal fragments show minor occurrences of preserved primary porosity that has not been occluded by calcite cements. In the Meramec, the skeletal grains that are not heavily micritized act as

nucleation sites for the early calcite cements that occlude primary intergranular porosity. These skeletal fragments are also a source of later calcite cements that occur following compaction and can be partially dissolved by stylolites. Unlike the Osage, the Meramec shows no signs of meteoric alteration.

Burial of the Meramec and Sycamore Shale Formations resulted in minor amounts of fracturing and the formation of overgrowths and secondary porosity. Quartz overgrowths developed following compaction and resulted in occlusion of intragranular porosity. The source of the Si for the overgrowths is thought to be transformation of clay material during illitization in mudstones at temperatures exceeding 90 $°$C (Thyberg et al., 2010). The overgrowths on quartz grains are observed cross cutting feldspars that contain secondary intragranular porosity. The pores within the feldspars and related clay minerals also contain bitumen linings. Therefore, hydrocarbon migration, illitization, and quartz overgrowths most likely occurred coeval during paragenesis.

Reservoir Quality

Reservoir potential is dependent upon many variables related to migration, storage, and recovery of hydrocarbons. Organic-richness, maturation, and fluid conduits are the most crucial factors for migration. Porosity and thickness are the main controls of hydrocarbon storage. Permeability as well as mechanical properties have become increasing important to understanding how to economically recover hydrocarbons. This study focused on visually characterizing porosity types, understanding fluid migration events, and characterizing mineralogic variations. One of the primary goals was to determine if certain lithologies had enhanced or diminished reservoir quality throughout the Osage, Meramec, and Sycamore reservoirs. An inverse correlation of calcite to porosity within the formations analyzed was first

understood by comparing lithofacies to well log data. Studies done by Drummond (2018) and

Duarte (2018) show a strong negative relationship between calcite abundance and total porosity

and a strong positive relationship between clay and total porosity. These studies also reported a

linear relationship of porosity and permeability meaning that these pores are well connected.

These observations required a quantitative method to relate lithofacies to mineralogy. Therefore,

chemofacies were created from HHXRF data. The following will discuss the perceived reservoir

quality of each lithofacies based on petrographic analysis and porosity models from well logs

and then will discuss the reservoir potential of each chemofacies based on its mineralogic

properties.

Sandy fossiliferous packstone (Figure 9): The sandy fossiliferous packstone shows very

minimal amounts of porosity related to the high concentration of carbonate cement. Minor

amounts of poorly connected porosity developed within skeletal fragments and peloids. Locally

calcite cement has been pervasively replaced with chert which contains micro-porosity. This

lithofacies is well cemented and highly indurated creating a very hard and brittle rock.

Calcitic siltstone (Figure 11): The calcitic siltstone is a carbonate facies lacking obvious

porosity. Porosity within this rock type occurs within the feldspars that have undergone

dissolution following calcite cementation. The calcitic siltstone contained abundant natural and

induced fractures, many of which were cemented with calcite.

Argillaceous Siltstone (Figure 12): This clay supported facies has a much higher storage

capacity than carbonate lithofacies. However, the pore types observed in the argillaceous

siltstone was primarily within clays that may not be efficiently connected. The fracturing

observed in this rock type terminate in intervals with increased clay content and reduced silt

and carbonate. Interbeds composed of highly brittle calcitic siltstones and more ductile

31

argillaceous siltstones results in a complex mechanical stratigraphy.

Bioturbated Siltstone (Figure 13): The bioturbated siltstone is the most porous interval observed in this study. This clay dominated facies is heavily bioturbated and this preserved primary intergranular porosity between silt grains by preventing calcite nucleation. The heterogeneity of this rock type develops planes of weakness that could lead to increased fracture complexity.

Silty Mudstone (Figure 14): Silty mudstones have a high clay content that results in an overall increased porosity related to interlayer clay pores. Also occurring in silty mudstone is an increase in organics that also contain organo-porosity. However, this lithofacies lacks obvious natural or induced fracturing in core implying increased ductility compared to other lithofacies.

Glauconitic Siltstone (Figure 15): The glauconitic siltstone occurs at the Woodford and Mississippi carbonate interface. This lithofacies is very thin and most likely has limited effects on reservoir quality in this system. However, this rock type should be considered during reservoir characterization for its ability to act as a fluid baffle or frac barrier because of its high clay content.

Argillaceous spiculite (Figure 8): The argillaceous spiculite facies has an elevated quartz content and increased interlayer clay porosity and porosity associated with organics. This spicule lithofacies is the most likely source of silica for the chert replacement of the carbonate facies.

Argillaceous mudstone (Figure 8): The argillaceous mudstone facies has the highest observed clay content and total porosity. However, it is difficult to determine how connected the pore systems are, and if recovery will be limited by this increase in clay content. However, Figure 28-A shows that the main clay type in the study area is mixed layer and/or illite clay

which is a brittle clay that should not impact fracture stimulation.

Clay dominant lithofacies are shown to have a high degree of anisotropy (Pj) and primarily an oblate texture (Figure 34). The clay rich chemofacies determined using quantitative XRF analysis support this trend (Figure 35). The increased clay content compared to the silt and carbonated dominated lithofacies is a result of decreasing detrital quartz and carbonate. This implies that clay textures are dependent upon framework grain (silt and carbonate detritus) concentration. The oblate petrofabrics observed in the clay rich facies represent the optimal mineral surface area for adsorption of organics (Parés, 2015). Heij (2018) showed a linear correlation between Pj and TOC implying an increased effective organo porosity and hydrocarbon potential. Therefore, the clay dominant facies with higher Pj could have increased reservoir potential.

Chemofacies 1 and 2 are the least porous chemofacies observed in this study with chemofacies 1 being the poorest quality reservoir. Chemofacies 3 and 4 are clay supported and have the highest concentration of the clay proxy aluminum. Chemofacies 3 and 4 contain concentrations of aluminum greater than 15,000 ppm. Therefore, using the previous correlations, chemofacies 3 and 4 are the most porous intervals. When considering the potential for these two facies to be source rocks, chemofacies 4 shows an increase in organic proxies Mo and V. These elements are proxies for anoxic bottom water conditions that preserve organics. However, this chemofacies has concentrations of aluminum up to 70,000 ppm with decreasing concentrations of silica and carbonate that would make the chemofacies brittle. This concentration of a clay proxy could limit the recovery of hydrocarbons because of its ductility. However, Figure 28-A shows that the main clay type is illite, a brittle clay. This clay type may limit the ductility, but more tests are needed to confirm the mechanical properties of these

formations. Therefore, chemofacies 3 shows the highest reservoir potential. Chemofacies 3

contains minor amounts of calcite that could occlude porosity, while maintaining the necessary

brittleness to develop natural and induced fractures to increase its potential hydrocarbon

recovery.

Constructing lithofacies and chemofacies is an important process for understanding

reservoir quality in the Osage, Meramec, and Sycamore Formations. Developing an

understanding of pore types and diagenetic alterations from core is crucial for understanding

reservoir potential. Once the lithofacies are understood, additional data can be collected on

cuttings to supplement reservoir characterization. Further, applying correlating these lithofacies

to well logs can be used to develop electrofacies that will allow for a better regional

characterization of lithologies throughout the system.

Conclusions

1. Reservoir quality is dependent on lithology for the Osage, Meramec, and

    Sycamore Formations within the STACK, MERGE, and SCOOP. Porosity,

    permeability, mechanical properties, and the extent of diagenetic alteration

    vary depending on lithology. The carbonate facies in the study area lack

    significant storage volumes unless they have been altered by meteoric

    diagenesis. The silt and clay supported facies contain porosity related to

    dissolution of unstable minerals, interlayer clay porosity, and organic porosity.

2. The Sycamore Limestone is the time equivalent to the Osage, and underwent

    similar depositional processes. Reduced accommodation space resulted in

    progradation into the deeper sections of the basin. Sedimentary structures from

    both formations as well as thickness trends show a northern source for the

Osage and a southern source for the Sycamore Limestone.

3. Upper portions of the Sycamore are the downdip equivalent of the Meramec and resulted from gravity flows and turbidity currents that resulted from processes occurring along the Anadarko Shelf. The Meramec in the STACK is much thicker than the Sycamore shale and has a higher amount of carbonate detritus.

4. Paragenesis of the Osage and Sycamore Limestone Formations is the result of near surface meteoric diagenesis that enhanced porosity through decalcification. Fracturing resulting from burial processes show evidence for hydrothermal fluid flow in the Anadarko Basin. The Osage and Sycamore Limestone was primarily an open system through geologic time.

5. Meramec depositional features such as clay coats and bioturbation have prevented calcite cement nucleation in the more clay dominant facies types and preserved primary porosity. However, the carbonate supported facies underwent rapid diagenetic alteration that cemented fossil fragments, silt grains, and peloids in sparite.

6. Hydrothermal alteration most likely occurred approximately coeval with hydrocarbon migration. Fracturing in the Sycamore Limestone contains baroque dolomite, hydrocarbons, and silica cement lining the fracture faces.

7. Porosity in the Osage and Sycamore limestone resulted from meteoric diagenesis. This process dissolved early carbonate cements developed enhanced secondary porosity.

8. AMS data shows a strong oblate fabric in the rock types that are clay-rich and

could increase organic adsorption capacity. Heavily cemented carbonate rocks contain a changing oblate to prolate fabric that is related to diagenetic alteration.

9. HHXRF is a useful tool for quickly and efficiently determining chemofacies that have high reservoir quality. Chemofacies 3 from this study has the highest reservoir potential with low calcium and moderate clay amounts that allow for storage and recovery.

The integration of stratigraphy, diagenesis, AMS, and HHXRF as well as traditional petrophysical analysis on unconventional reservoirs can provide critical understandings for characterizing unconventional reservoirs. These methods are efficient as well as non-destructive and result in a multiscale understanding of reservoir dynamics.
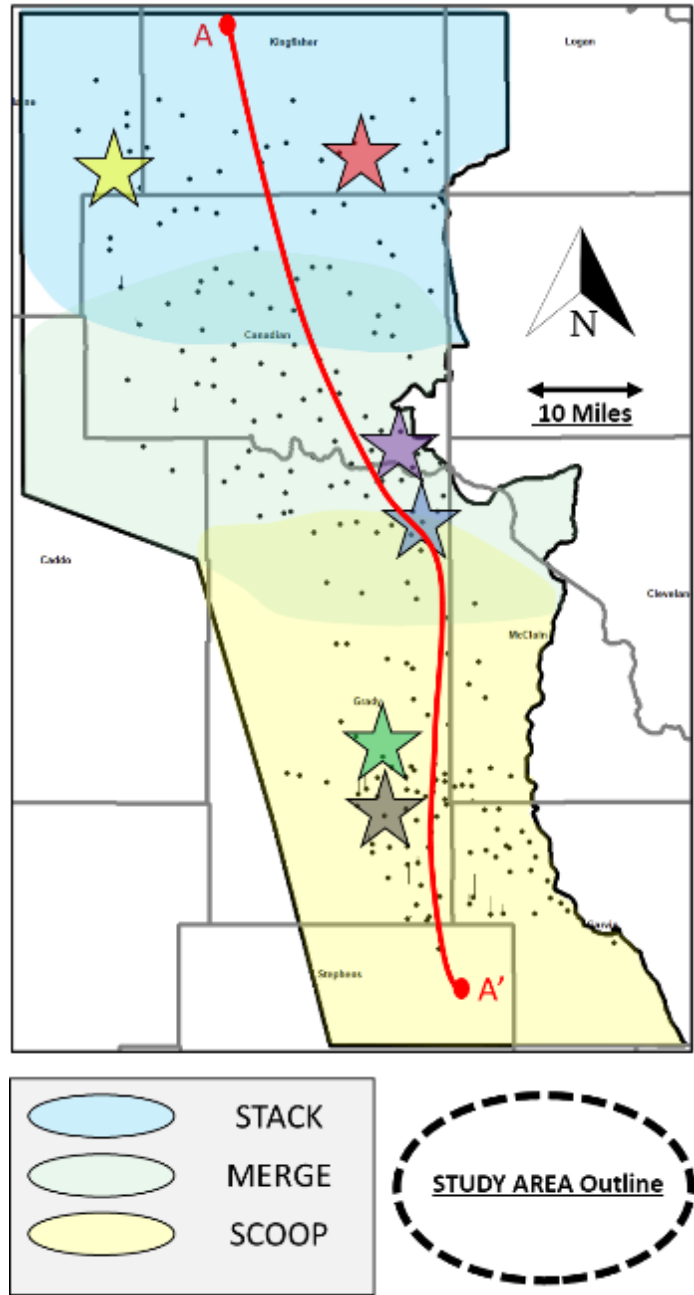
Figures

Figure 1—Base map showing study area of interest STACK, MERGE, SCOOP. Black dots represent wells with digital LAS curves that were used for petrophysical calculations. Red line represents cross section from STACK to SCOOP in Figure 37. Stars represent cores that were collected. Yellow star represents location of Schaeffer 1-23 (API: 35011215220000); red star represents location of Lloyd L Hawkins #1 (API: 35073300060000); purple star represents location of Payne #1 (API: 35017225520000); blue star represents location of Skaggs Ranch #1-9; green star represents location of Chitwood Harris #1 (API: 35051500910000); gray star represents location of core "X".

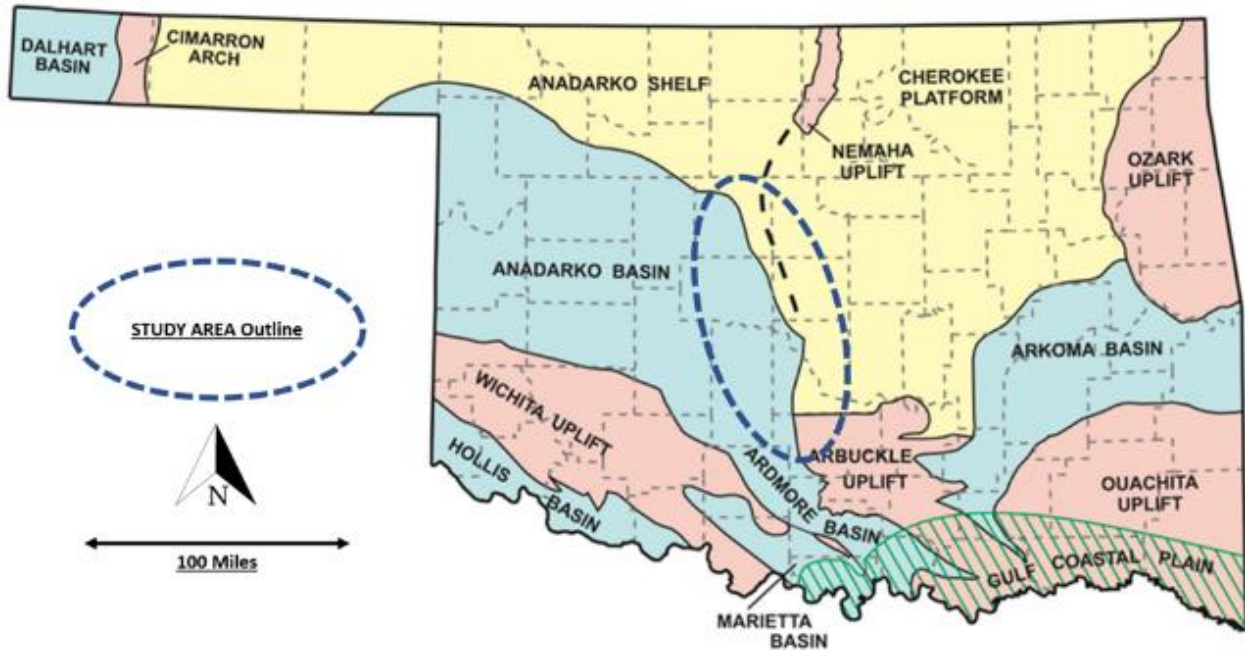**Figure 2—Major geologic provinces of Oklahoma (modified from Northcutt & Campbell, 1995)**
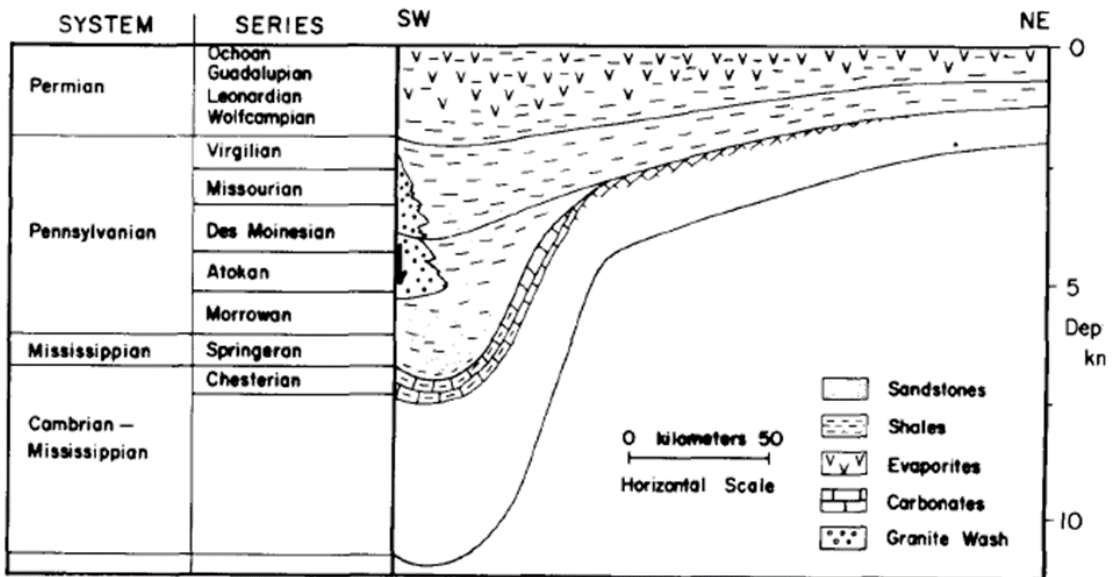
Figure 3—Cross-section perpendicular to the axis of the Anadarko basin. Over 12 km of sediment has been deposited in accommodation space created by thermal subsidence (Cambrian-Mississippian) crustal thinning (Mississippian to Late Des Moines) and flexure of the elastic lithosphere (Des Moines-Permian) (Garner & Turcotte, 1984)
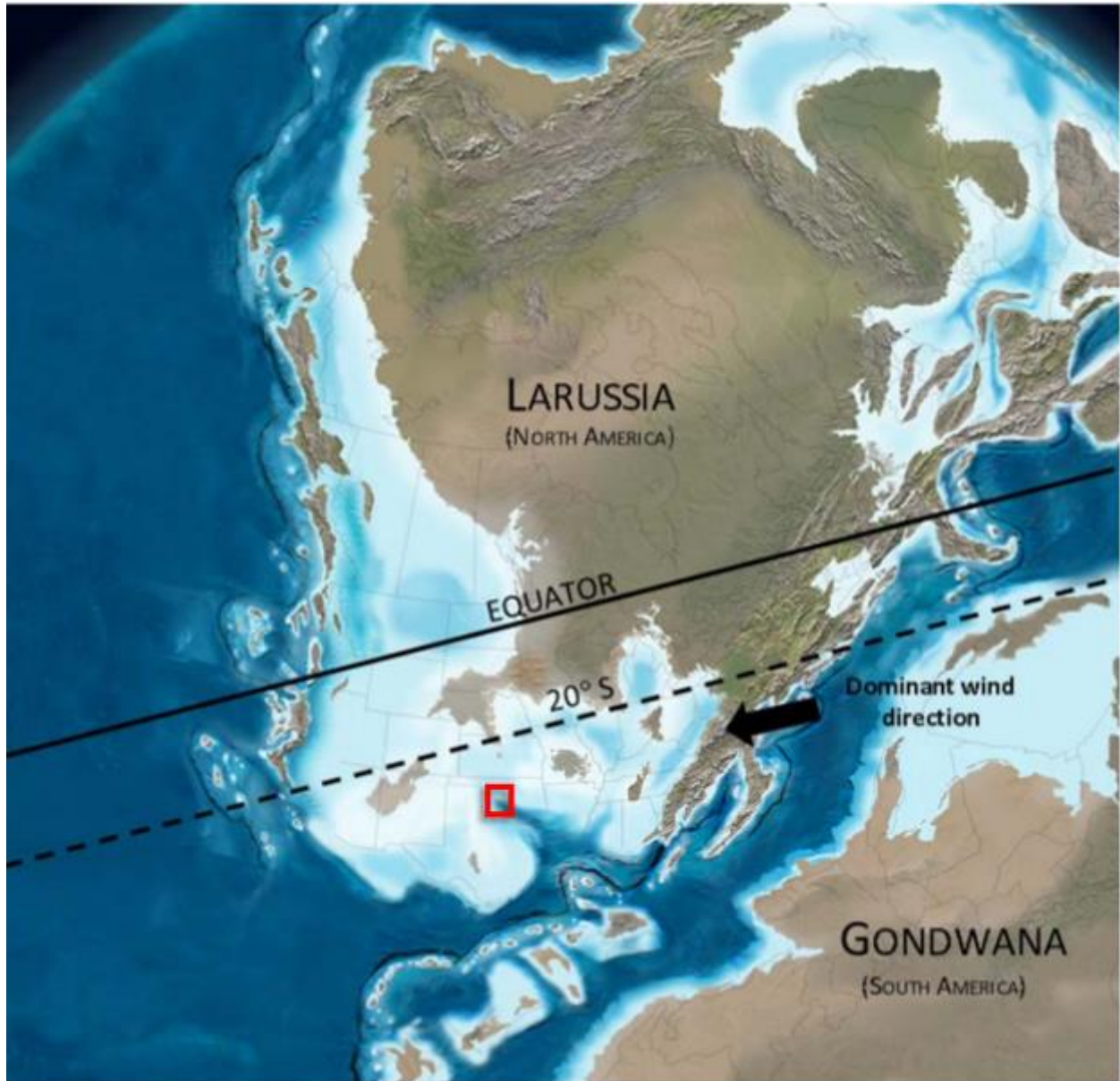
Figure 4— Paleogeographic map of the Early Mississippian. The study area is located in the Anadarko Shelf. Warm shallow sea covered the study area with prevailing wind and current direction coming from the present day northeast direction. The study area is highlighted in red (Modified from Blakey, 2013; Price, 2014).
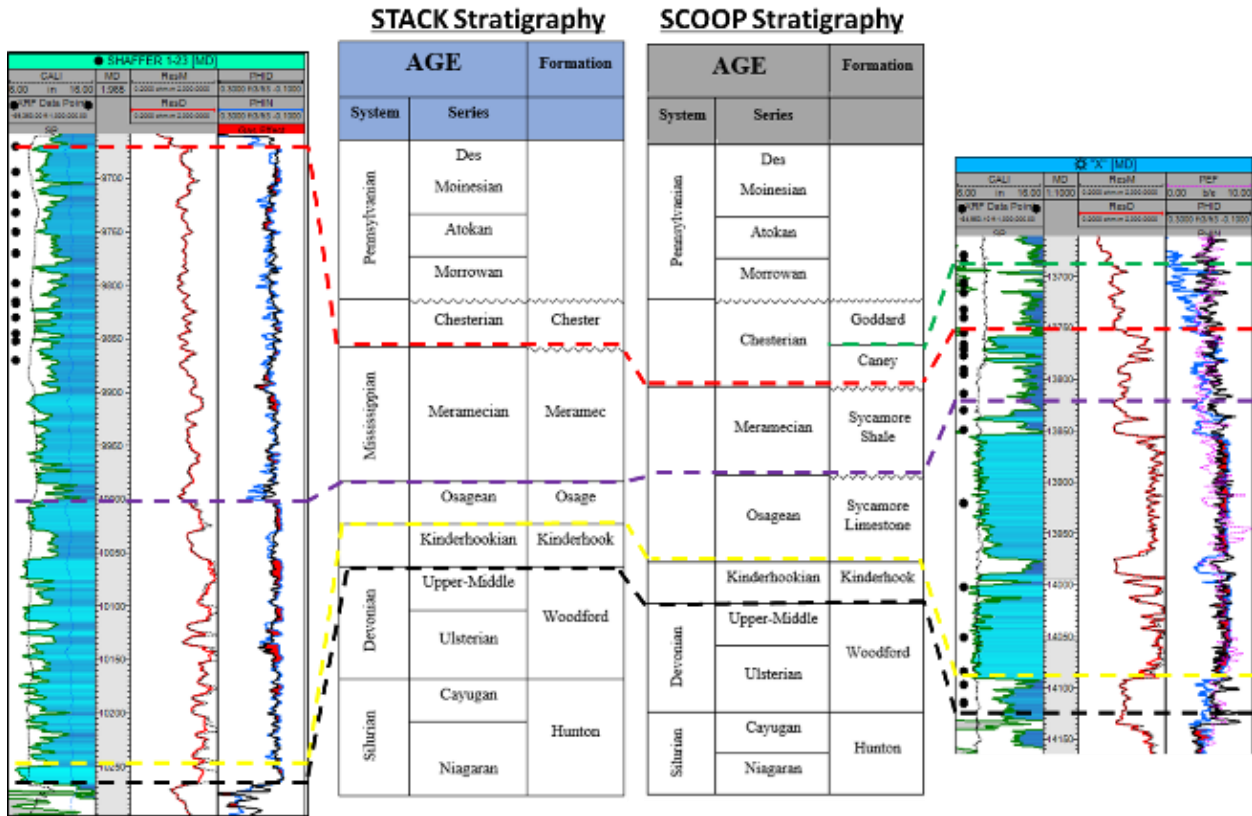
Figure 5—Stratigraphic framework for both STACK and SCOOP areas of interest. STACK Meramec correlates to SCOOP Sycamore Shale. Osage correlates to Sycamore Limestone (modified from Johnson & Cardott, 1992; Boyd, 2008).
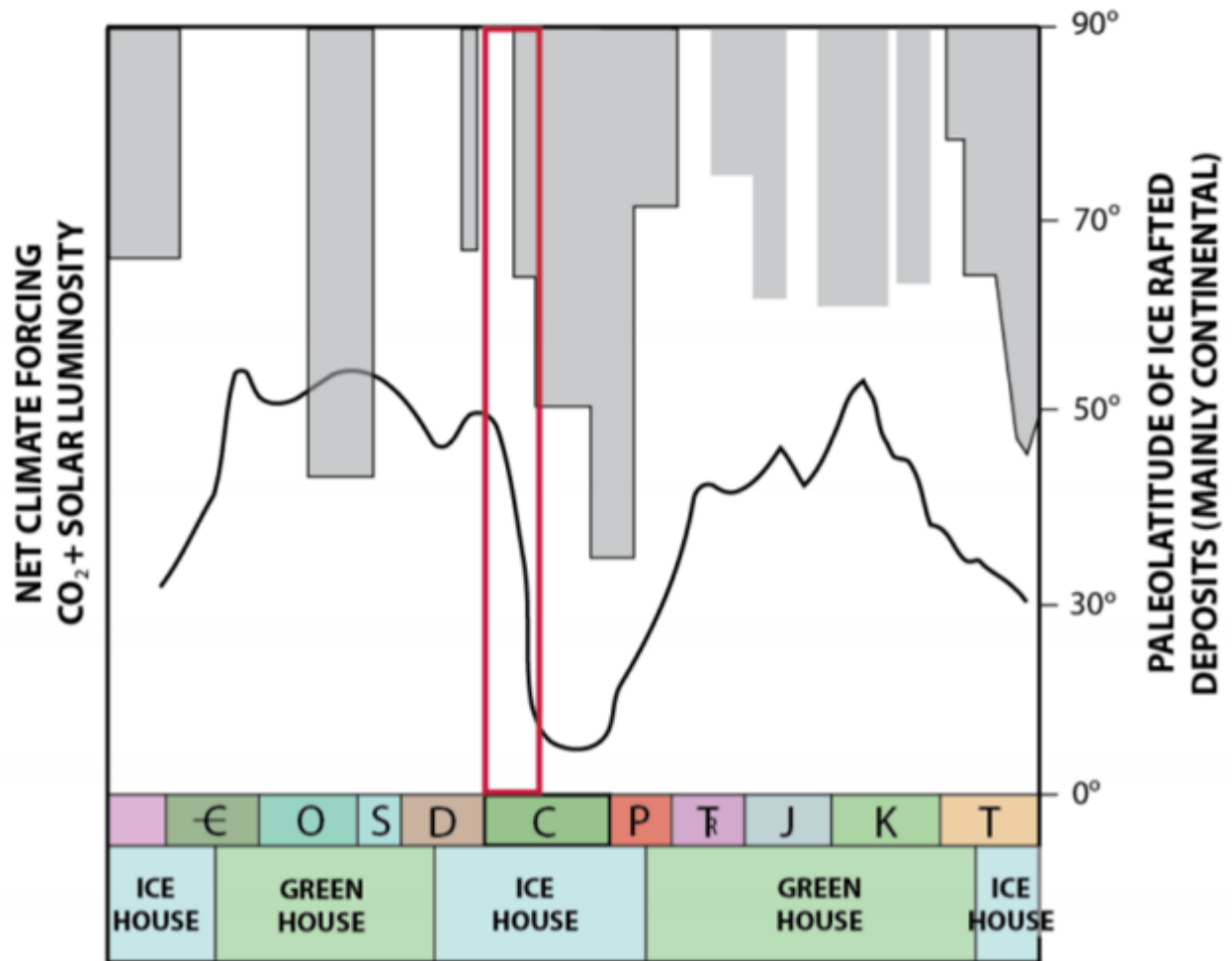
Figure 6—Distribution of icehouse and greenhouse periods during the Mississippian period. The Mississippian marks the transition between the Devonian greenhouse and Pennsylvanian icehouse (Price, 2014).
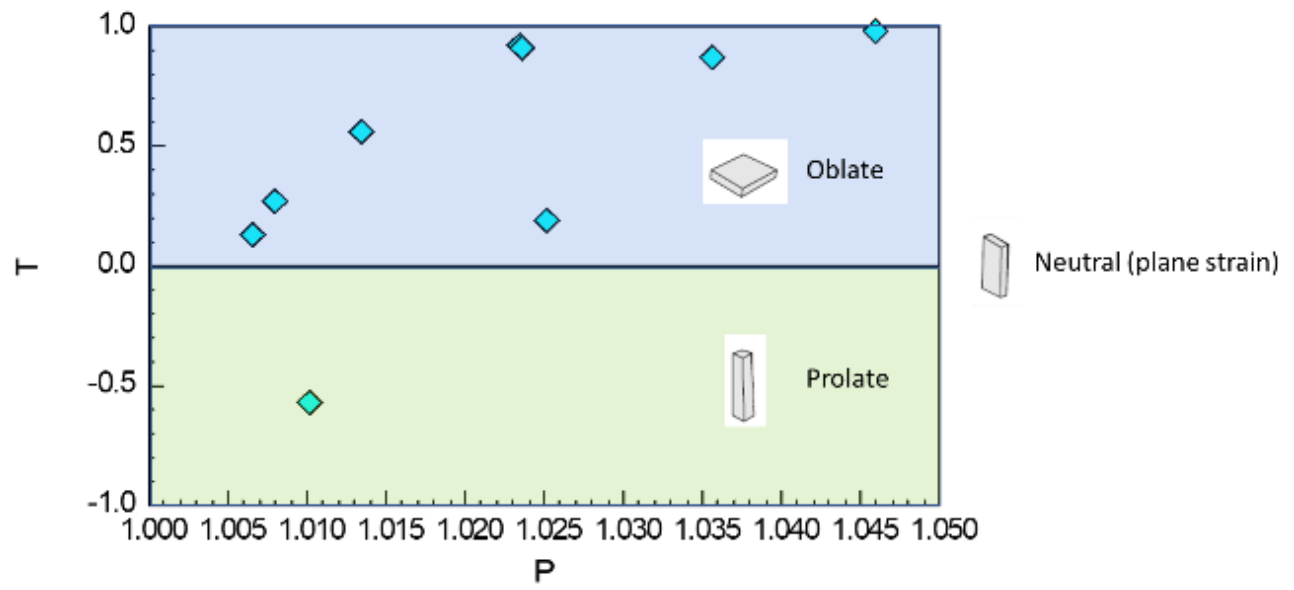
Figure 7—Example distribution of oblate and prolate fabrics on a Jelinek plot (modified from Dubey, 2014).
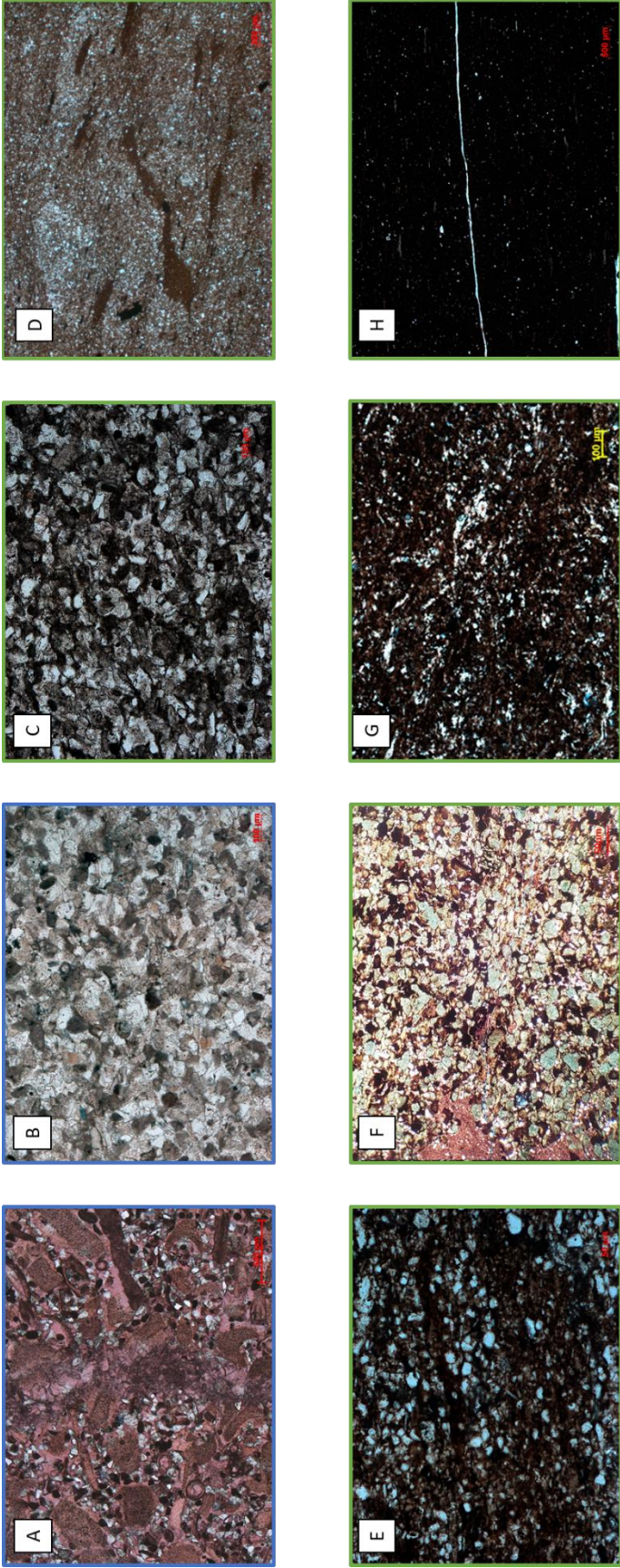
Figure 8—Overview of the facies analyzed in the study area. (A) Sandy fossilifeous packstone in CPL with calcite stained red by alizarin red. (B) Calcitic siltstone in PPL. (C) Argillaceous Siltstone in CPL with clay supported matrix. (D) CPL photomicrograph of the Bioturbated Siltstone. (E) CPL photomicrograph of the Silty Mudstone. (F) PPL photomicrograph of the Glauconitic Siltstone. (G) PPL photomicrograph of the Argillaceous Spiculite. (H) PPL photomicrograph of the Argillaceous Mudstone.
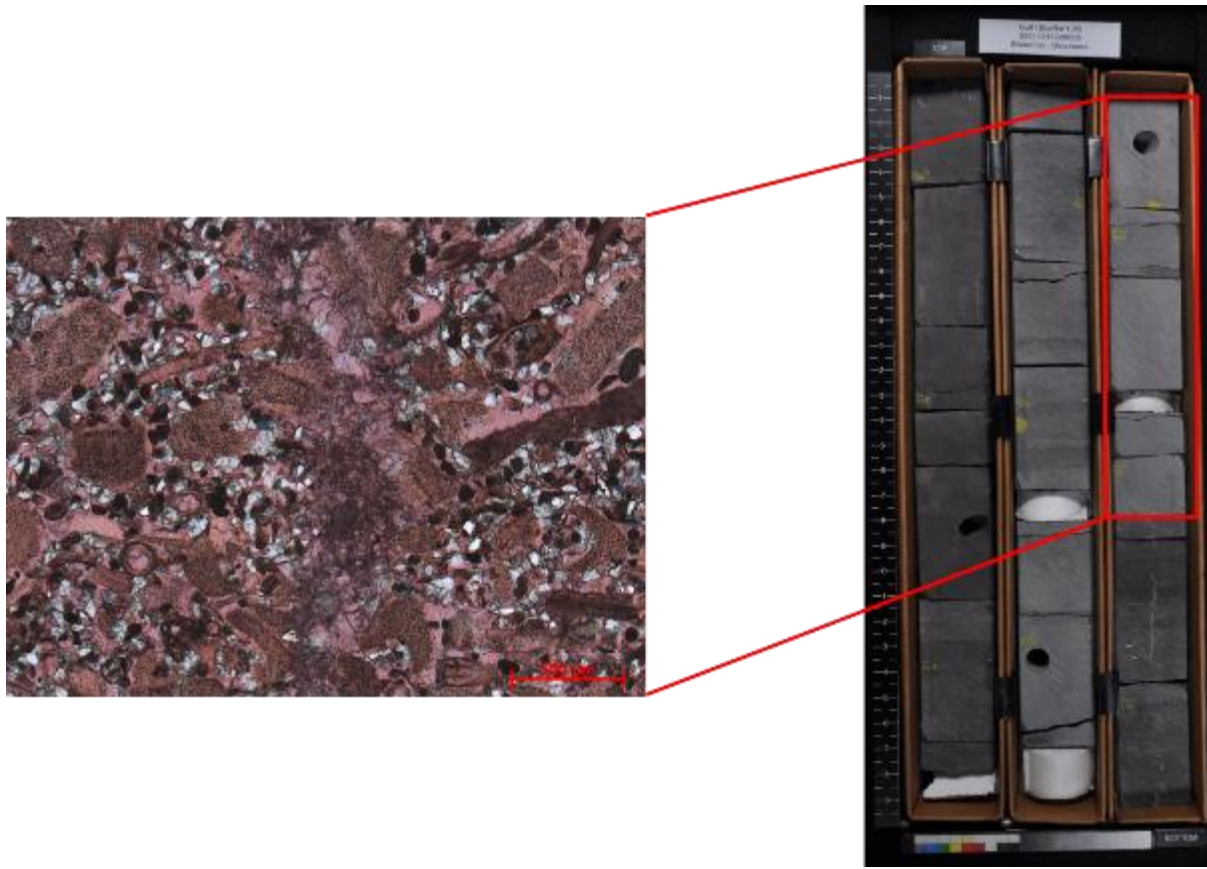
Figure 9—Sandy fossiliferous packstone facies in thin section (left) and whole core (right).
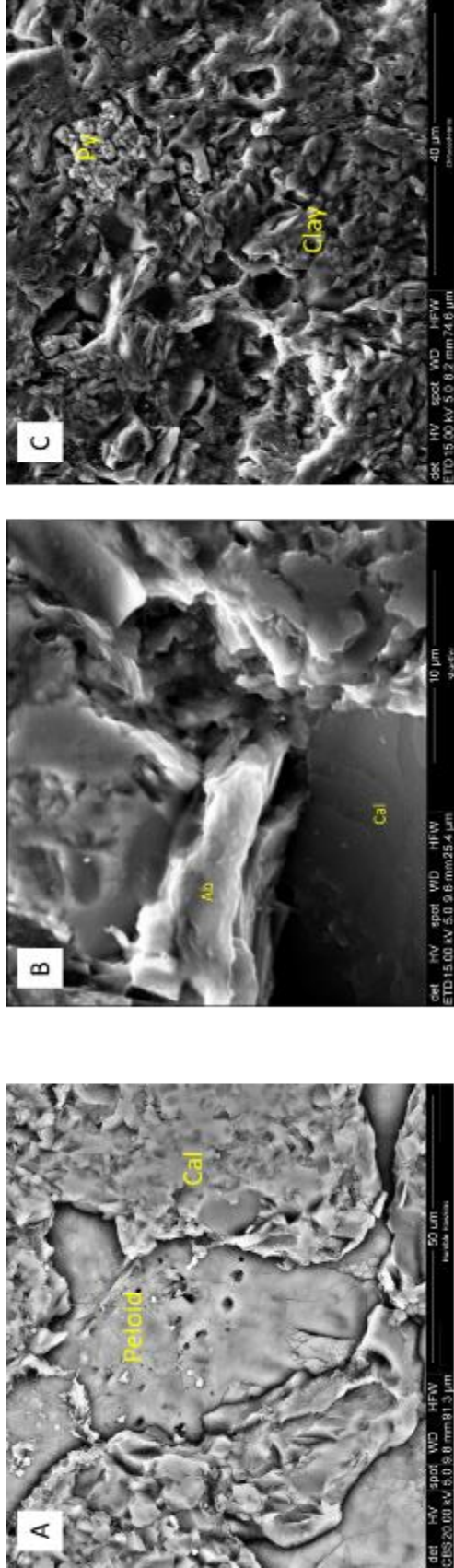
Figure 10—Porosity types seen in SEM. (A) porosity observed in the sandy fossiliferous packstone within a peloid surrounded by microporous chert. (B) Feldspar (Albite) dissolution resulted in porosity in a calcitic siltstone. (C) Example of porosity associated with clay and framboidal pyrite in an argillaceous siltstone.

Figure 11—Calcitic siltstone in thin section (left) and whole core (right).

Figure 12—Argillaceous siltstone in thin section (left) and whole core (right).
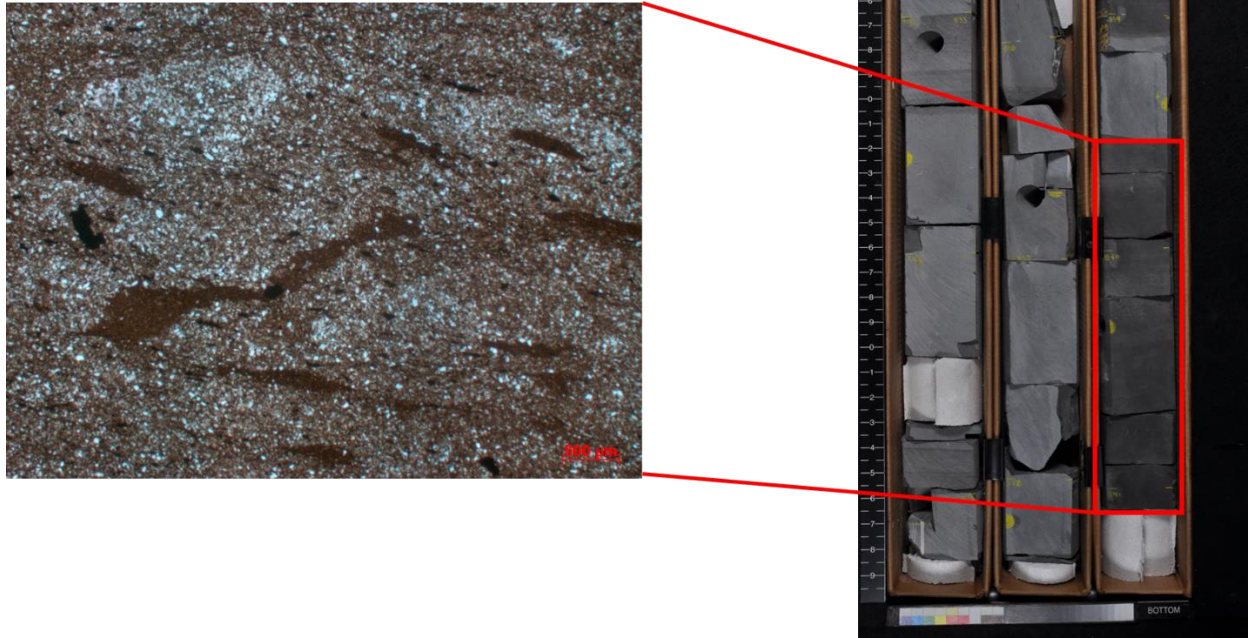
Figure 13—Bioturbated siltstone in thin section (left) and whole core (right).
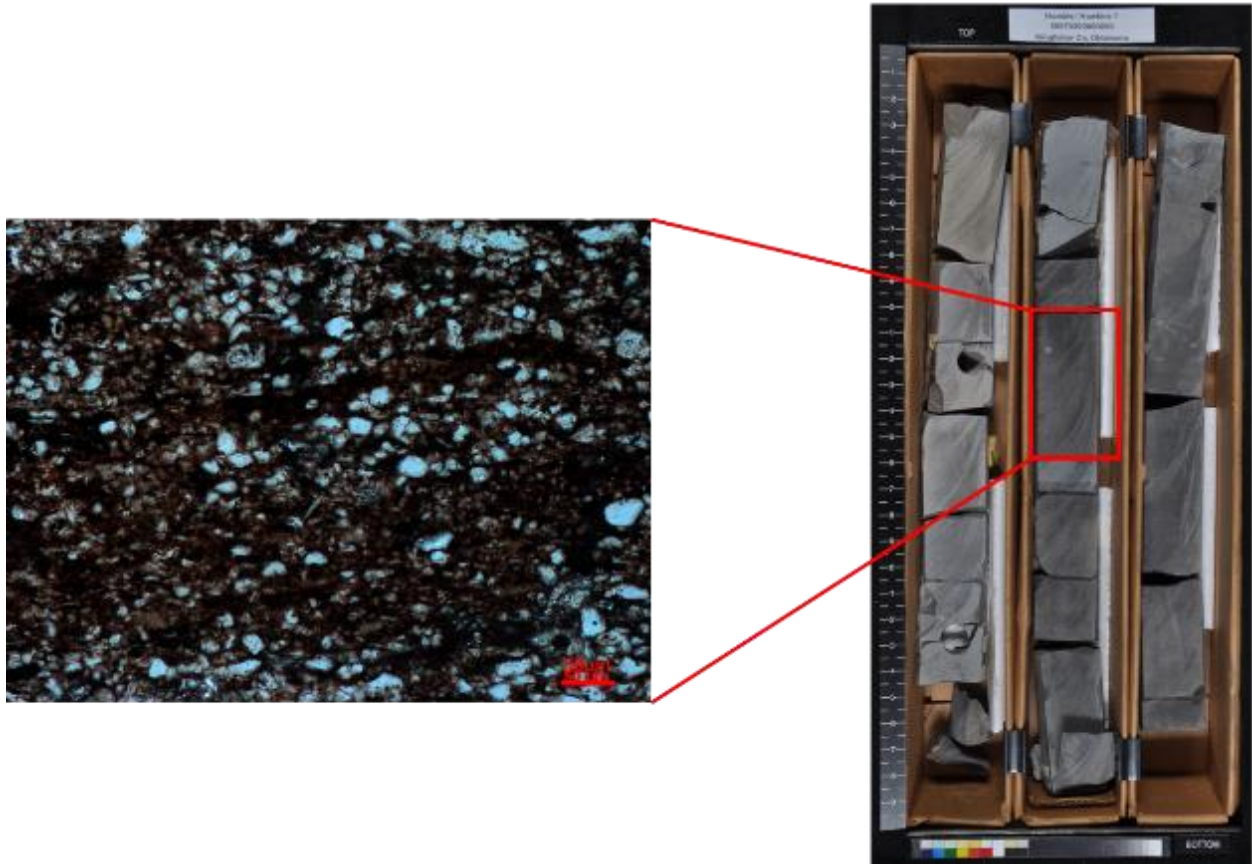
Figure 14—Silty Mudstone in thin section (left) and whole core (right).

Figure 15—Glauconitic siltstone in thin section (left) and whole core (right).

Figure 16—Open hole logs of the Meramec, Osage, and Woodford Formations from the Lloyd L Hawkins #1 from the STACK study area (Figure 1). Lithofacies and core points shown in right track. Thin sections and core based lithofacies were observed and XRF data were acquired over the Woodford Formation, but were not used for this study.

Osage Paragenetic Sequence

Event	Early ————————————————————————— Late
Micritization	▬▬▬
Pre-Compactional Veining	▬▬▬
Bioturbation	▬▬
Calcite Cement	▬▬▬
Spicule Dissolution	▬▬
Chertificiation	▬▬▬ ▬▬
Silica Dissolution	▬▬
Dolomite	▬
Dedolomite	▬
Mega Quartz	▬
Baroque Dolomite	▬
Hydrocarbon Migration	▬
Cubic Pyrite	▬
Fracturing	▬

Figure 17—Osage paragenetic sequence constructed from petrographic analysis of cross cutting and textural relationships that gives the relative timing of diagenetic events.
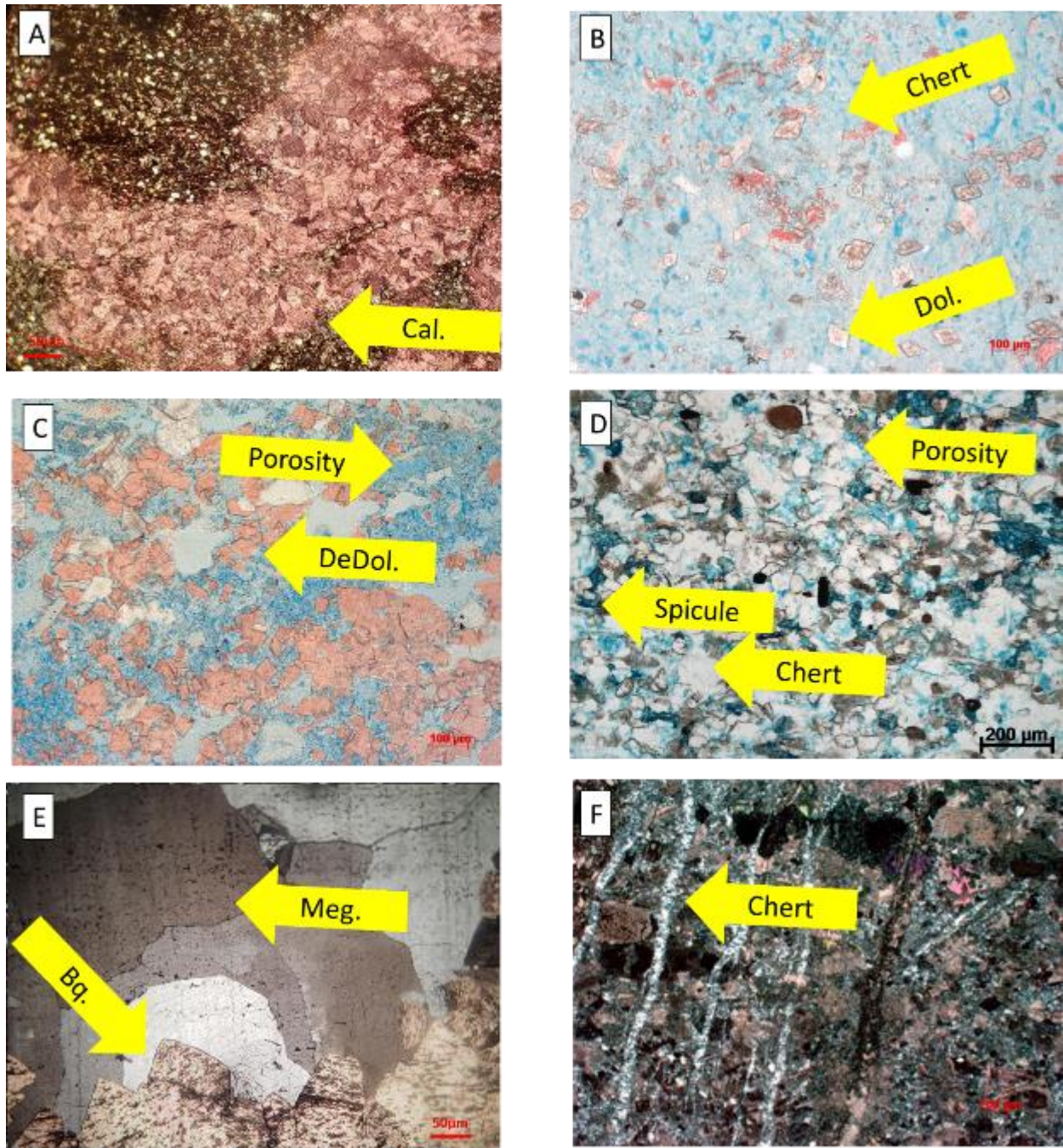
Figure 18— Photomicrograph A is a precompactional calcite cemented fracture. Photomicrograph B is is a silica replaced carbonate with dolomite that has been unaltered by chertification. C shows dedolomite occuring with the microporus chert implying a later calcium rich fluid flow event that dedolomitized the dolomite. D shows signs of sponge spicule dissolution and silica cementation around framework grains. E is a photomicrograph of fracture fill of mega quartz (Meg.) and baroque dolomite (Bq.) implying hydrothermal alteration. F is a fracture system that has been occluded with chert.
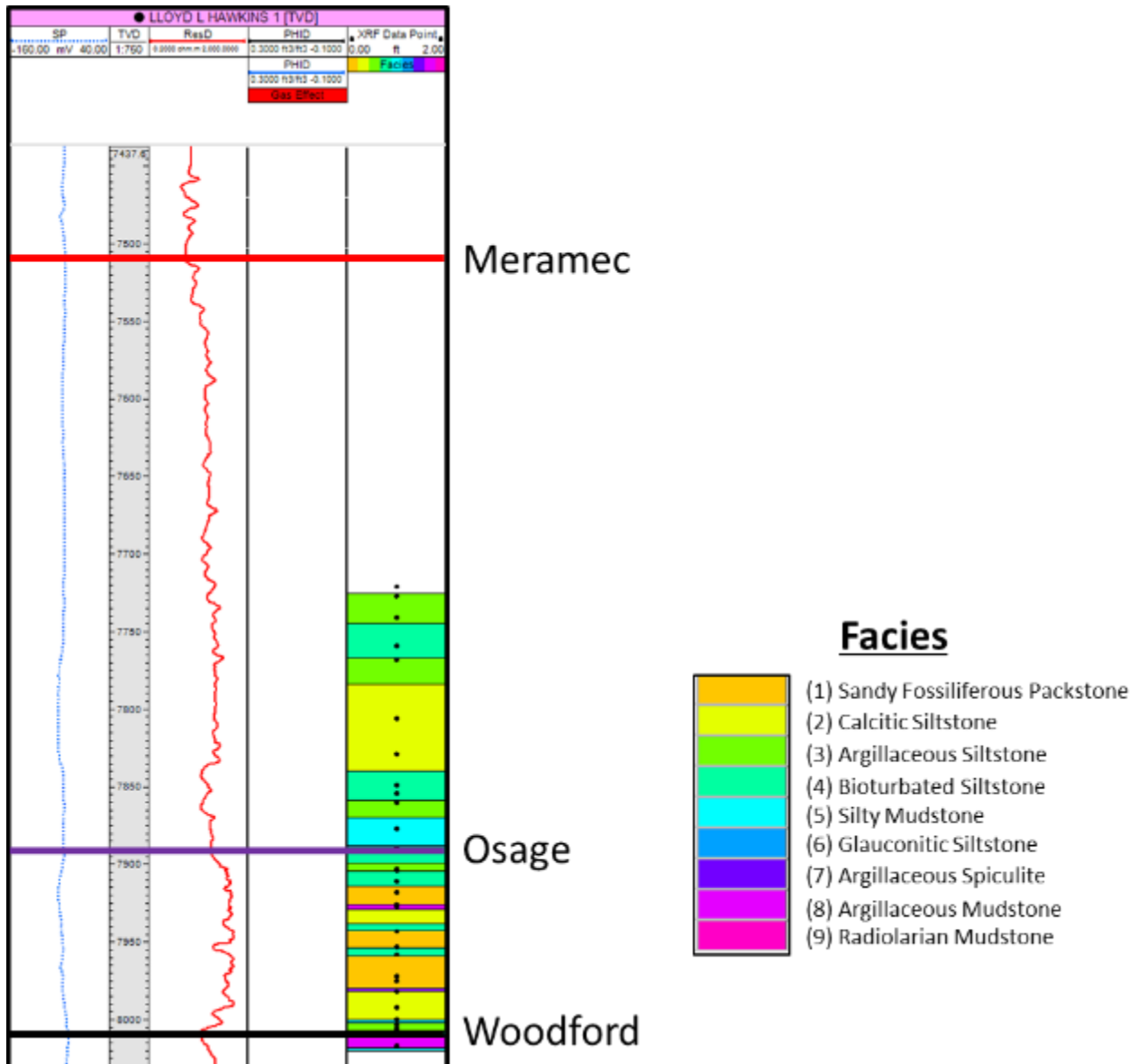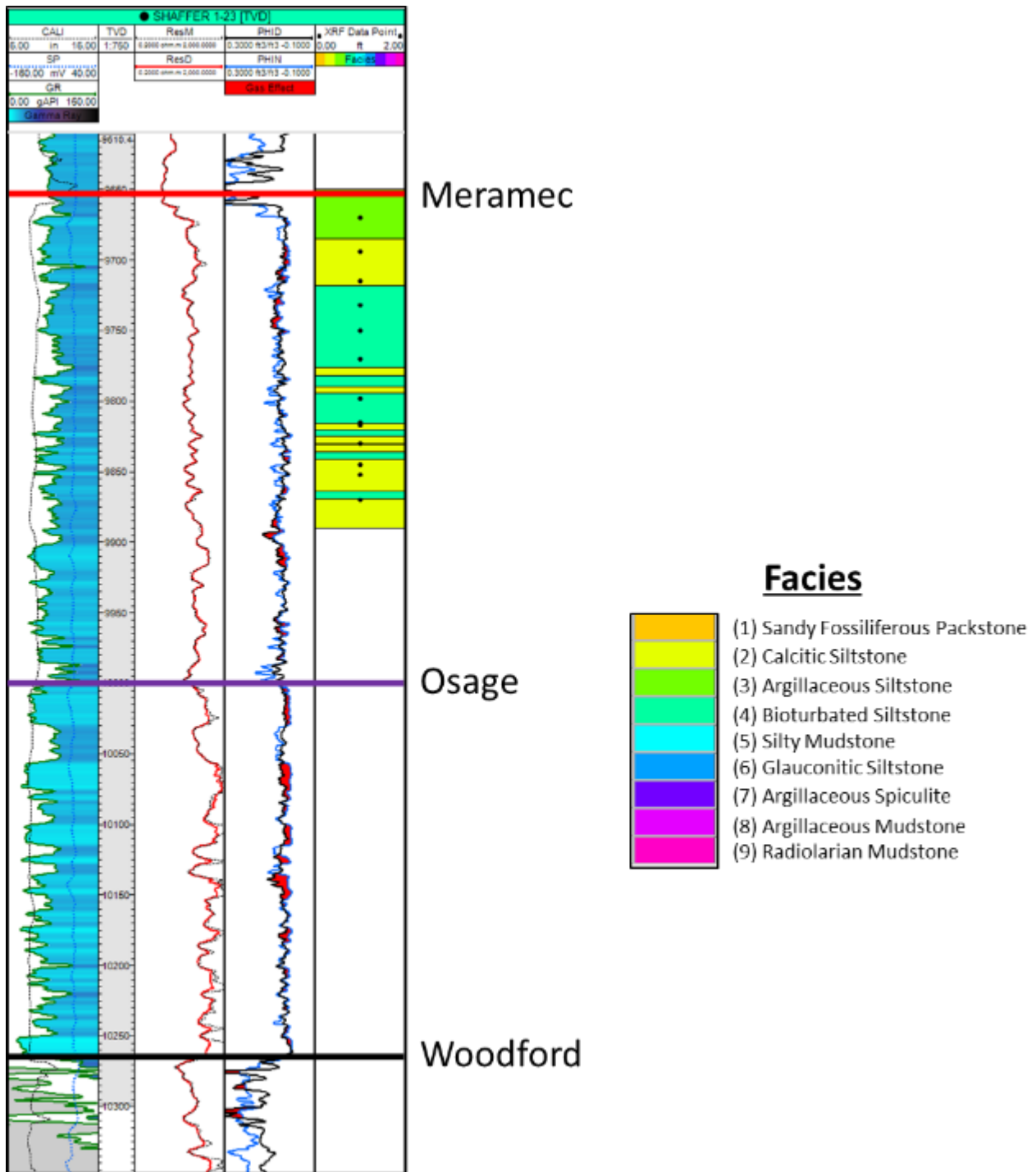
Figure 19—Open hole logs of the Meramec, Osage, and Woodford Formations from the Schaeffer #1-23 from the STACK study area (Figure 1). Lithofacies and core points shown in right track.
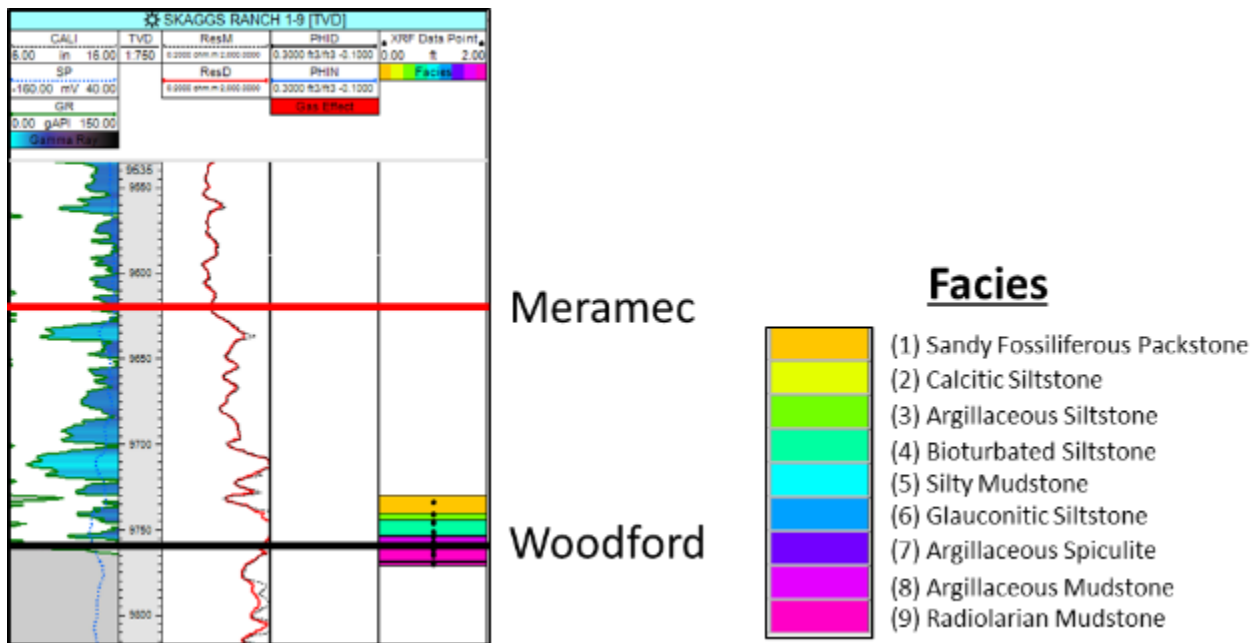
Figure 20—Open hole logs of the Meramec and Woodford Formations from the Skaggs Ranch #1 from the Merge portions of the study area (Figure 1). Lithofacies and core points shown in right track. Thin sections and core based lithofacies were observed and XRF data were acquired over the Woodford Formation, but were not used for this study.
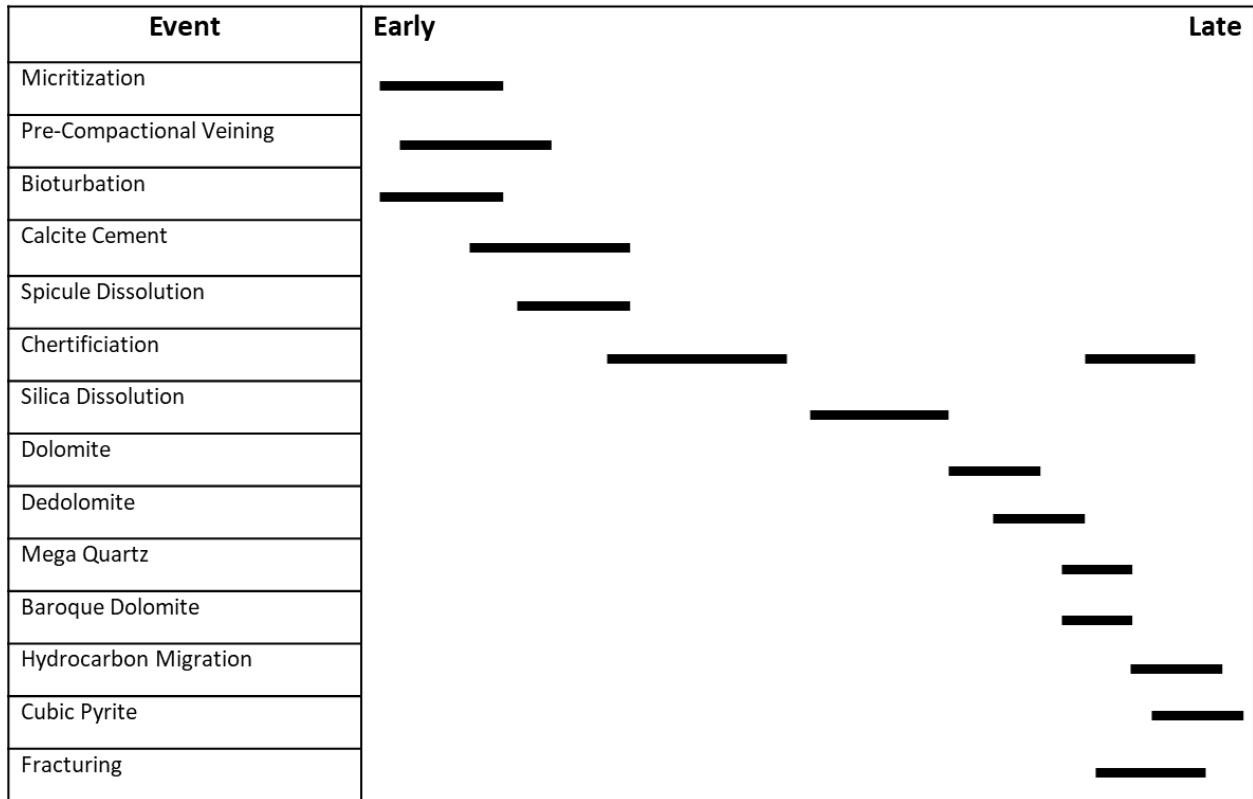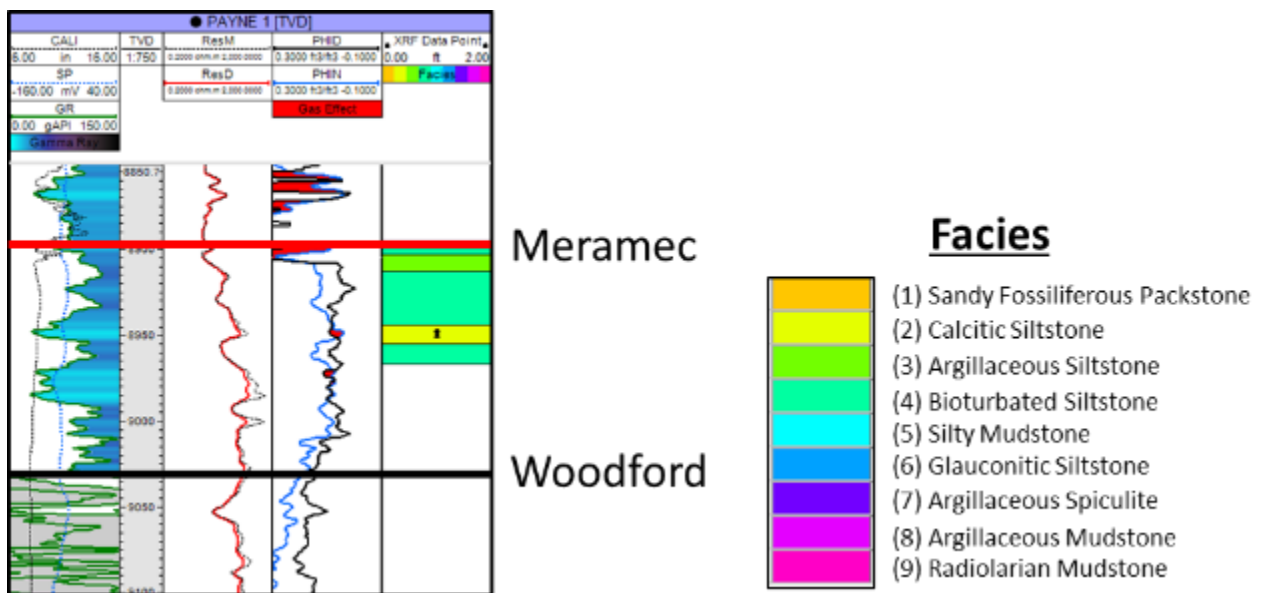

Figure 21—Open hole logs of the Meramec and Woodford Formations from the Payne #1 from the Merge portions of the study area (Figure 1). Lithofacies and core points shown in right track.

Meramec Paragenetic Sequence

Event	Early									Late
Micritization	▬									
Bioturbation	▬									
Framboidal Pyrite	▬									
Calcite Cement		▬						▬		
Compaction			▬▬▬							
Styolitization			▬▬▬							
Silica Overgrowths					▬					
Fracturing						▬				
Feldspar dissolution								▬		
Hydrocarbon Migration								▬		
Cubic Pyrite									▬	
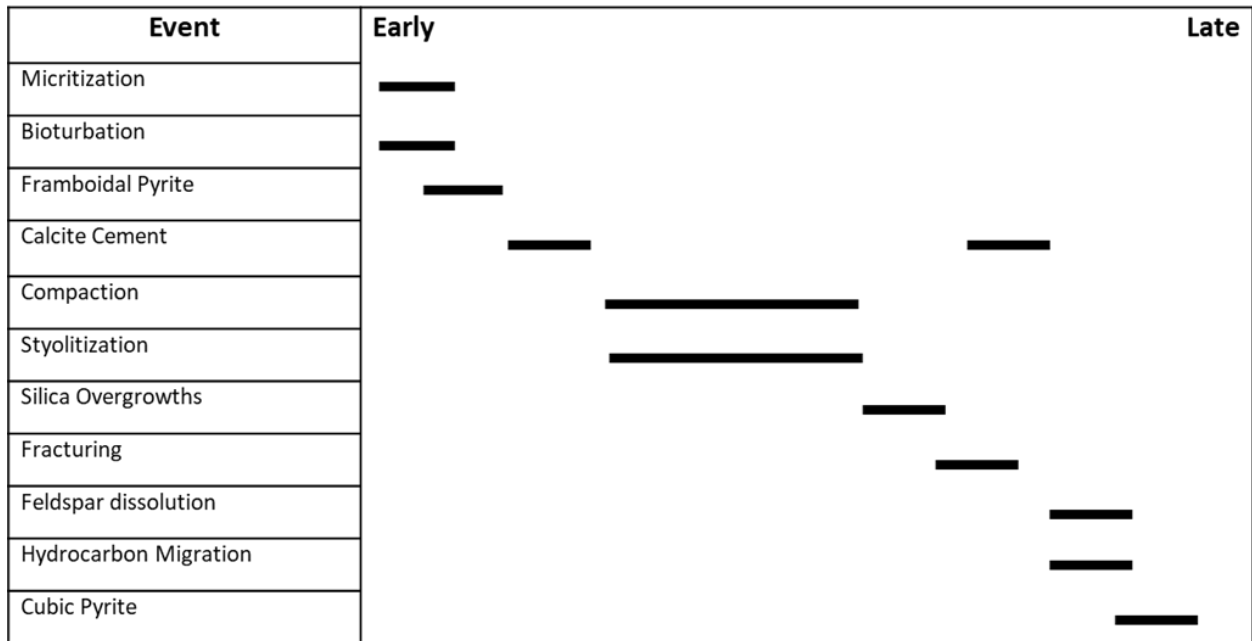
Figure 22—Meramec paragenetic sequence dominated by authigenic phases within the matrix and a later fracturing event that shows mineralization by calcite cementation.
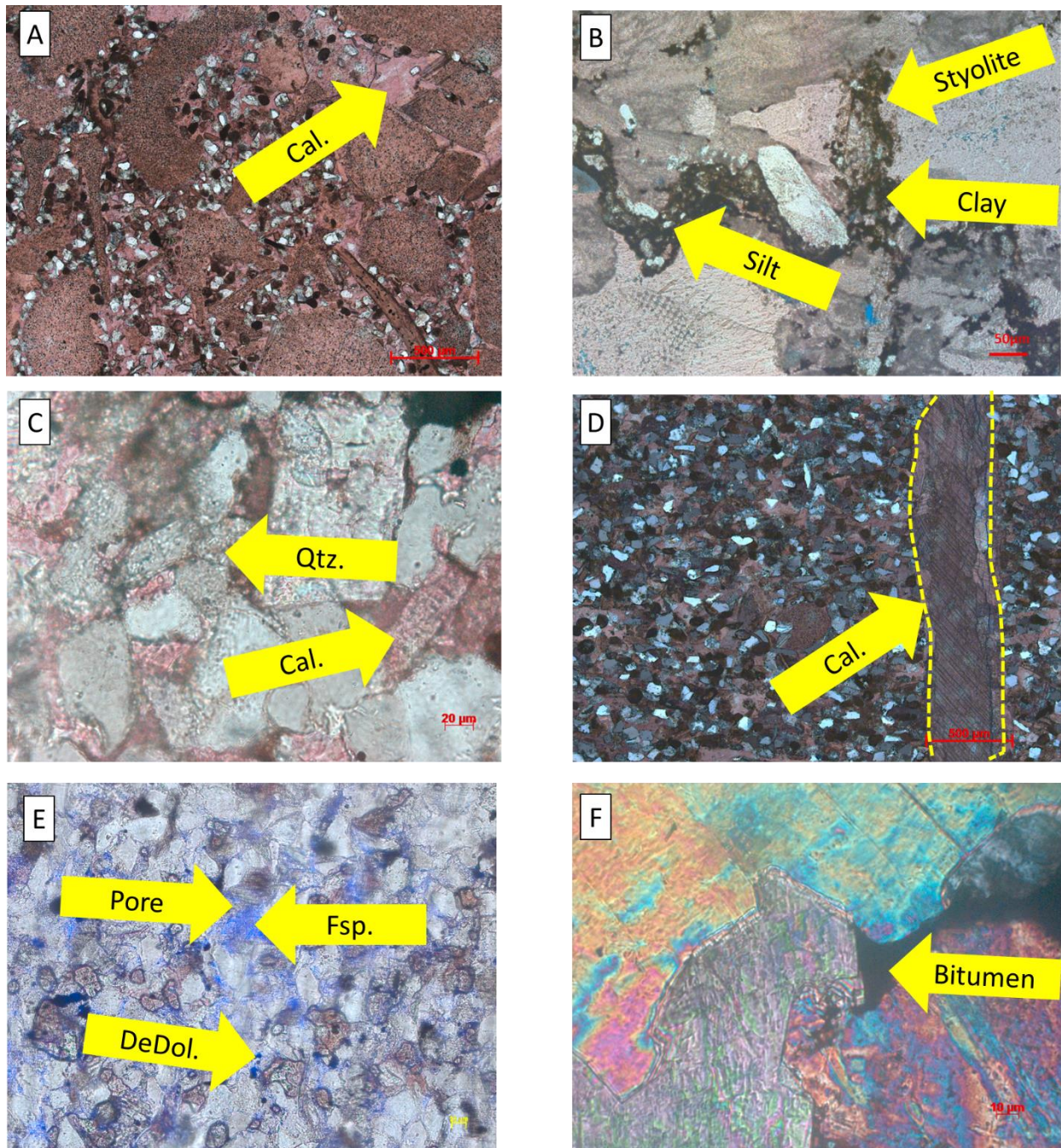
Figure 23—Primary authigenic features within the Meramec formation. Early calcite (Cal.) cement occludes intergranular porosity in photomicrograph A. Calcite stained by Alizarin red. Fractures that cross cut early diagenetic features are mineralized with calcite in photomicrograph B. Feldspars (Fsp.) are being dissolved and produce intragranular porosity and clay minerals in photomicrograph C. Photomicrograph D shows a styolite with clay residue and detrital silt grains. Quartz overgrowths between silt grains is occluding primary porosity in photomicrograph E. Photomicrograph F shows bitumen between dissolved calcite and dolomite grains.
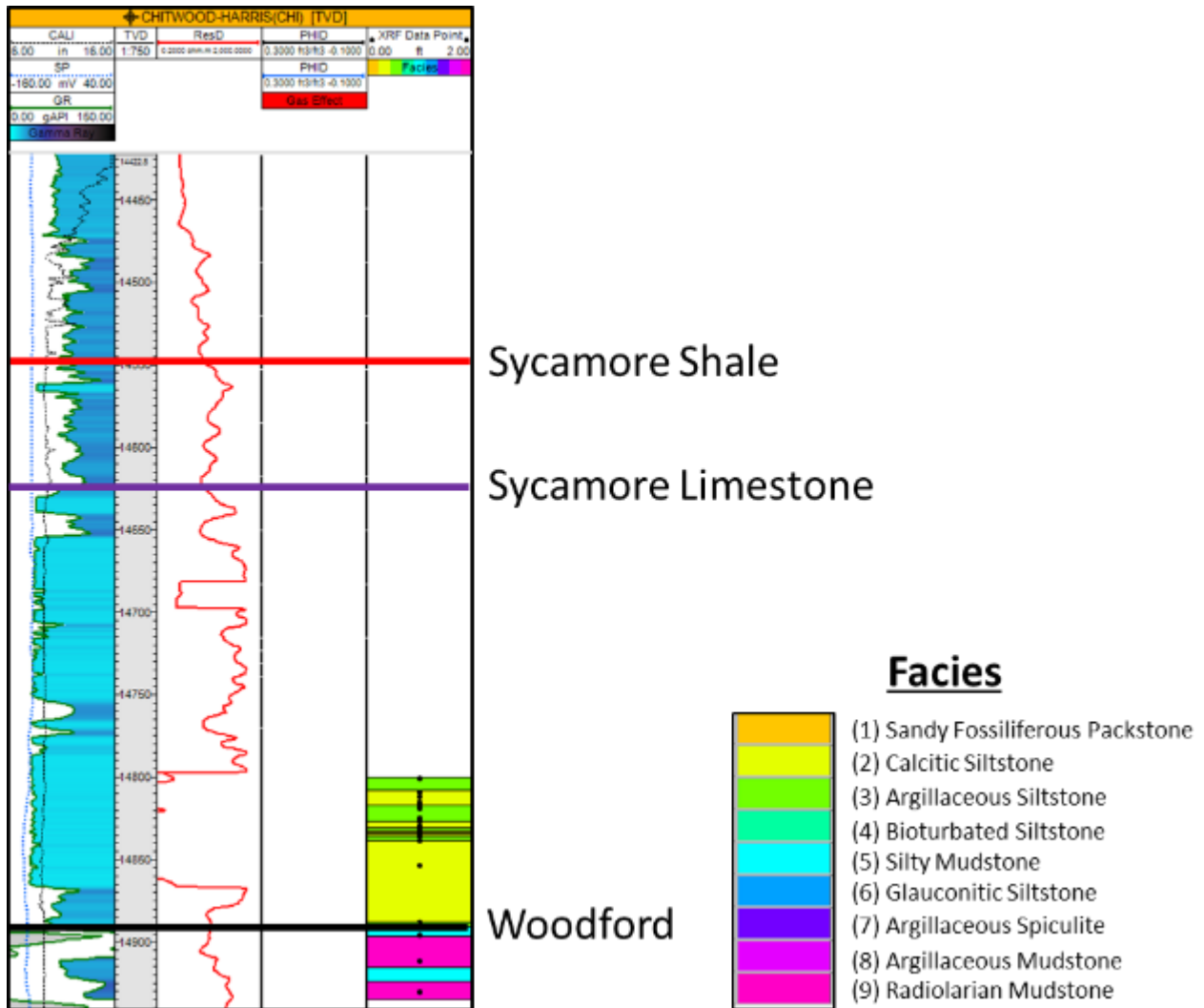
Figure 24—Open hole logs from the Sycamore and Woodford Formations acquired within the Chitwood-Harris #1 in the SCOOP portion of Grady County (Figure 1). Lithofacies and core points shown in right track. Thin sections and core based lithofacies were observed and XRF data were acquired over the Woodford Formation, but were not used for this study.
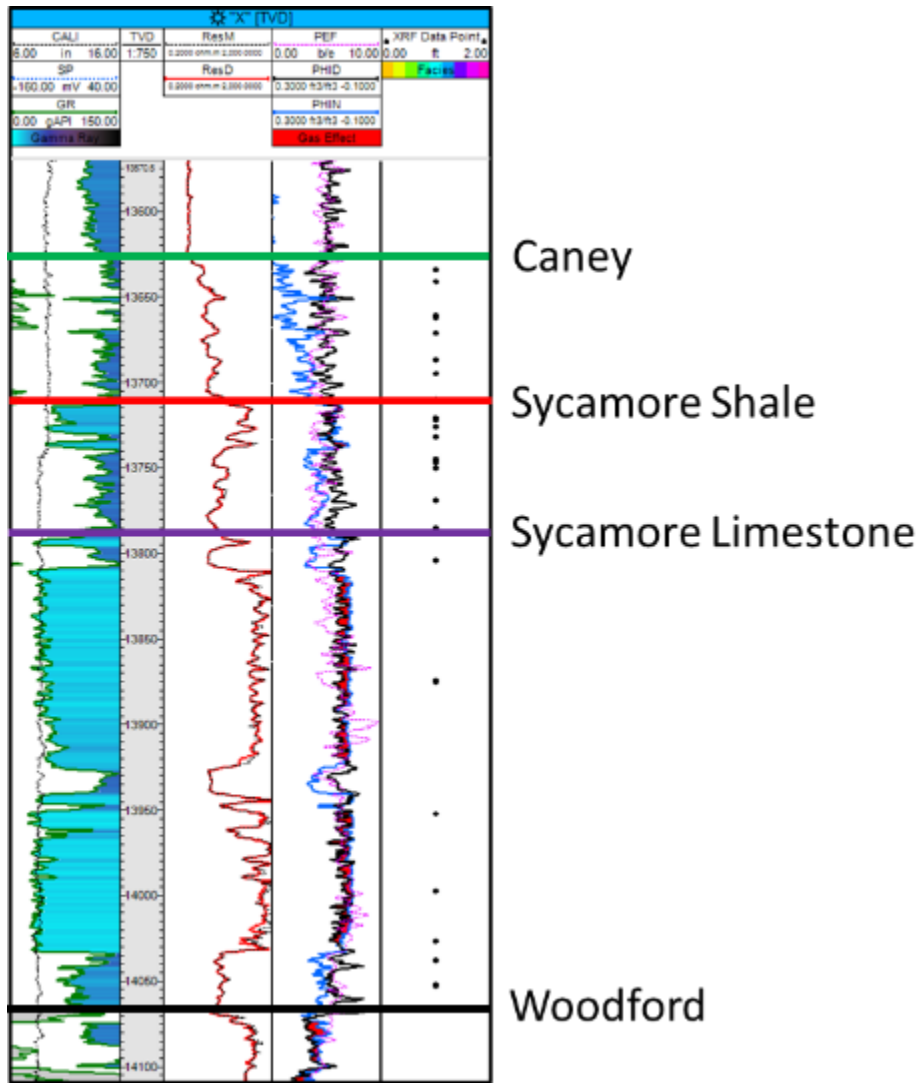
Figure 25—Open hole logs acquired from well "X" in the SCOOP portion of the study area within Grady County. The well logs cover the Caney, Sycamore, and Woodford Formations. Plugs from the Caney were also analyzed, but were not used for this study. Thin section based lithofacies were only acquired for this well. Therefore, a lithofacies description between thin section points is not supplied.

Sycamore Paragenetic Sequence

Event	Early ——————————————————————————————— Late
Calcite Cement	▬▬ ▬▬▬ ▬▬
Dolomite Cement	▬▬ ▬▬
Bioturbation	▬
Pre-Compactional Veining	▬▬
Framboidal Pyrite	▬▬
Aragonite Inversion	▬▬
Compaction	▬▬▬
Styolitization	▬▬▬
Fracturing	▬▬▬ ▬▬▬
Silica Cementation	▬▬ ▬▬
Mega Quartz	▬▬
Baroque Dolomite	▬▬
Dedolomitization	▬▬▬
Hydrocarbon Migration	▬▬▬
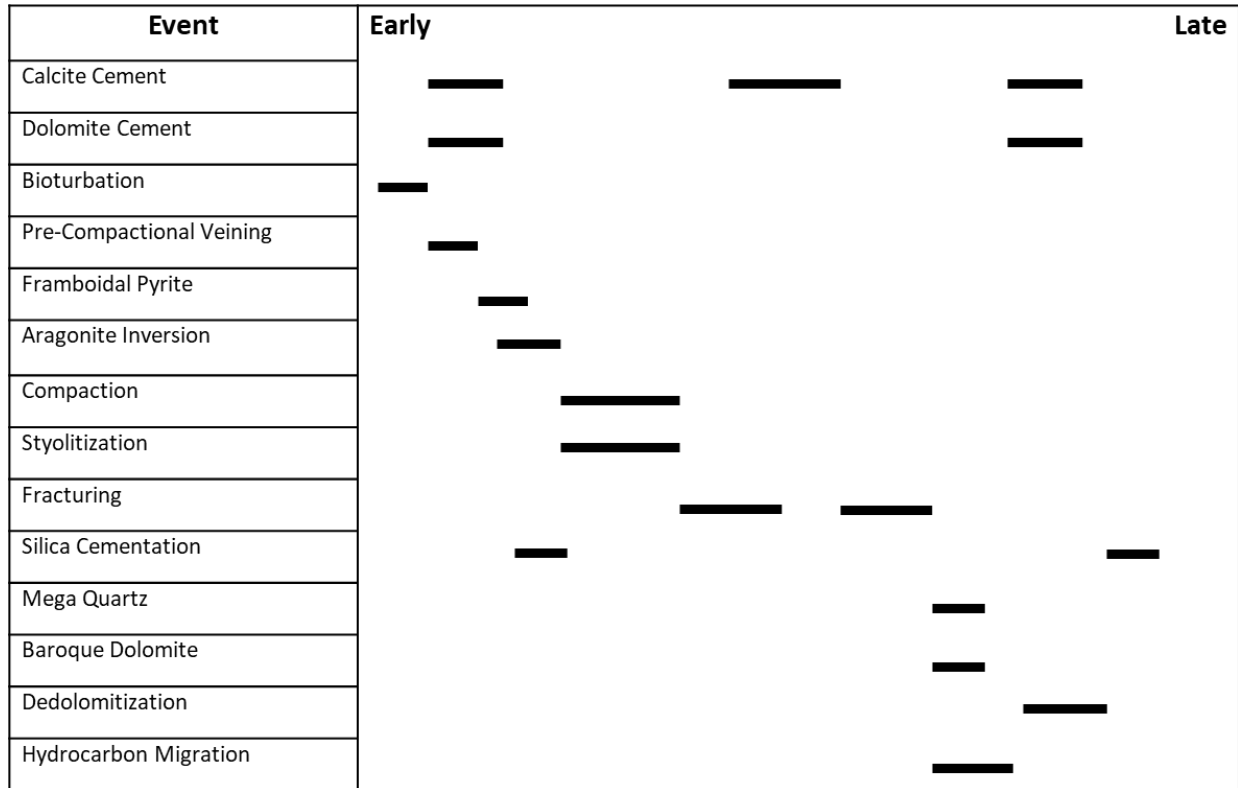
Figure 26—Sycamore paragenetic sequence composed of near surface cement precipitation, compactional features, and intense fracturing with multiple generations of fracture occluding cements.

60
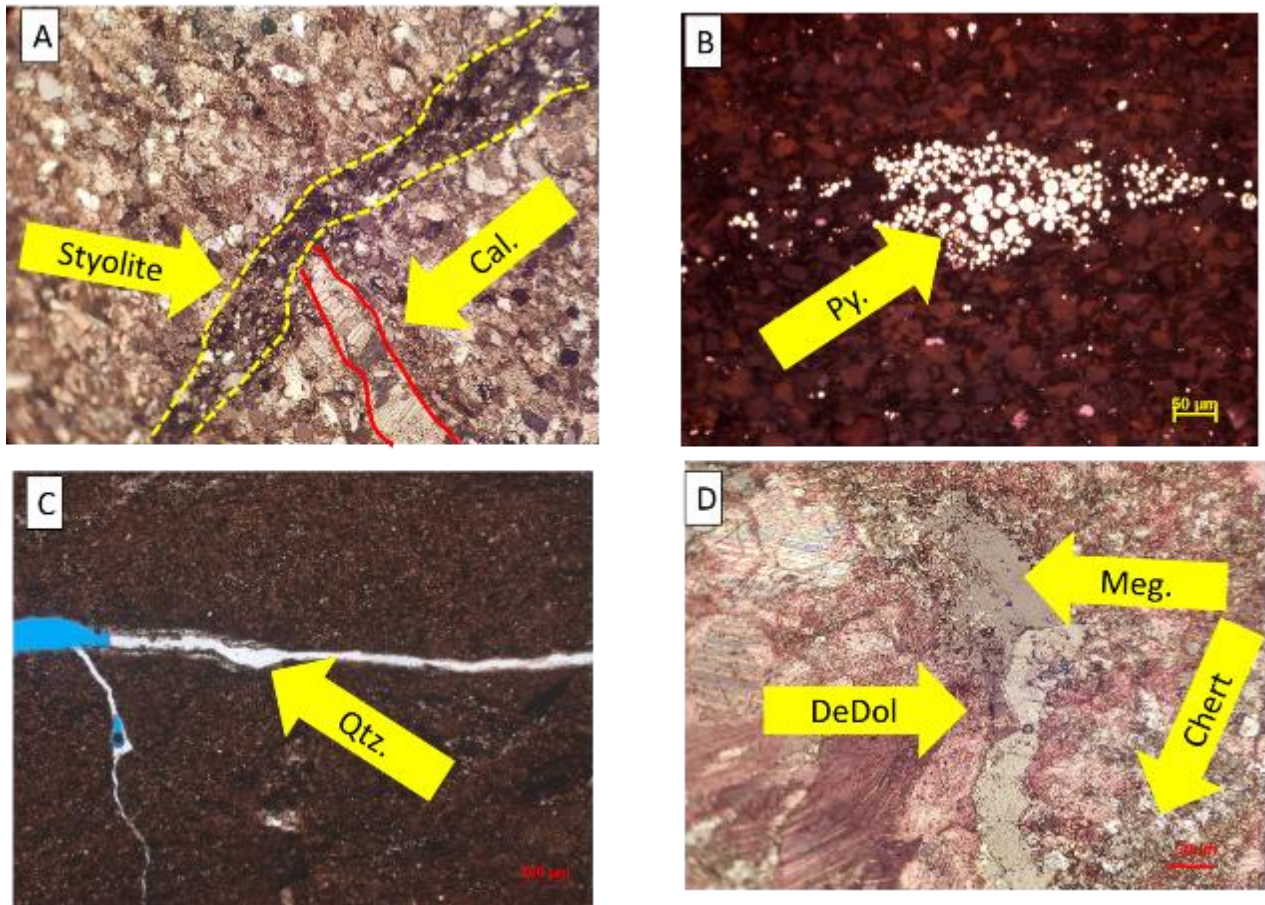
Figure 27— Photomicrograph A is a pre-compactional vein that is mineralized with calcite (Cal) cement and had been cross cut by a stylolite that resulted from chemical dissolution. Photomicrograph B is framboidal pyrite (Py.) in reflected white light that formed after initial calcite cementation. Photomicrograph C is a bifurcating fracture lined with baroque dolomite and hydrocarbons that has been replaced by silica cement (Qtz.). Photomicrograph D is a fracture with mega quartz (Meg) that is cross cut by dolomite that was then dedolomitized (DeDol). Within the matrix of photomicrograph D is chalcedony (chert) cement that is filling porosity within carbonate.
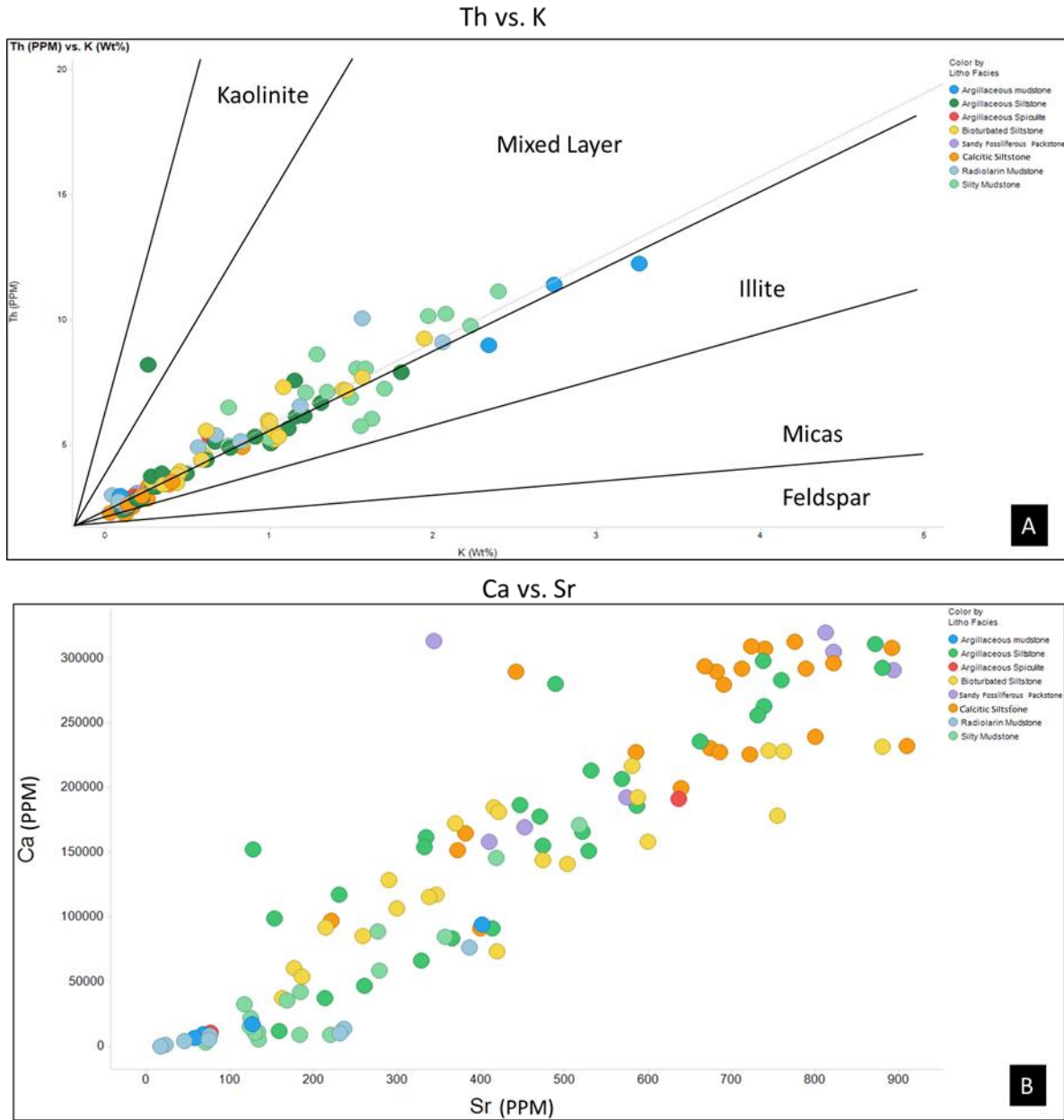
Figure 28—(A) Clay mineral typing from HHXRF using the ratio of Th (ppm) to K (wt.%). The data primarily plots in the mixed layer and portions of the graph. (B) Comparison of Ca vs. Sr shows strong linear correlation that is not facies dependent. Each facies show a linear gradational range of elemental abundance.
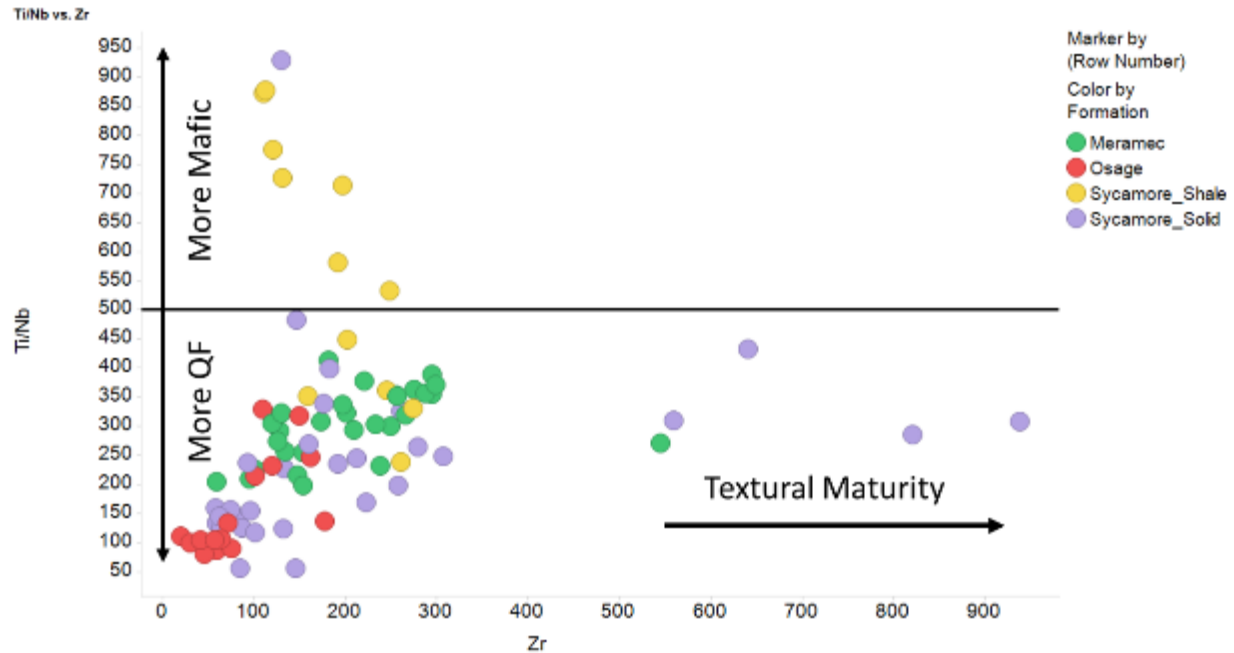
Figure 29— Ti/Nb ratio vs. Zr depicts 3 clusters of data related to provenance. The Data cluster above the Ti/Nb>500 is interpreted to be a mafic sourced rock. The cluster of Ti/Nb<500 is interpreted to be a more quartzofeldspathic source. The data with a higher Zr abundance (Zr>500) is interpreted to be from an inter basinal source that was reworked (Bonjour & Dabard, 1991; Heij, 2018).
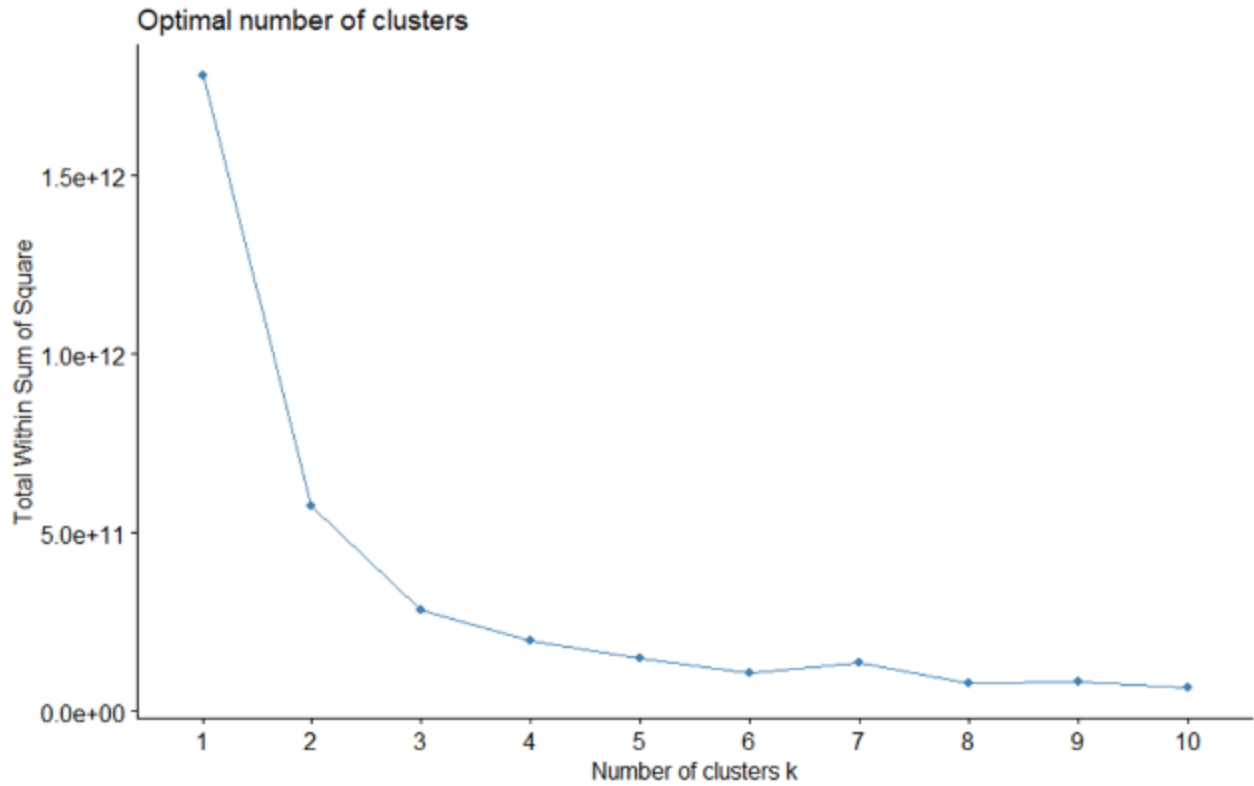
Figure 30— Elbow plot sum of squares of the clustered data to the number of clusters. Four clusters is the inflection point at where the variability in the total sum of squares decrease and there is limited variability after this number of clusters.
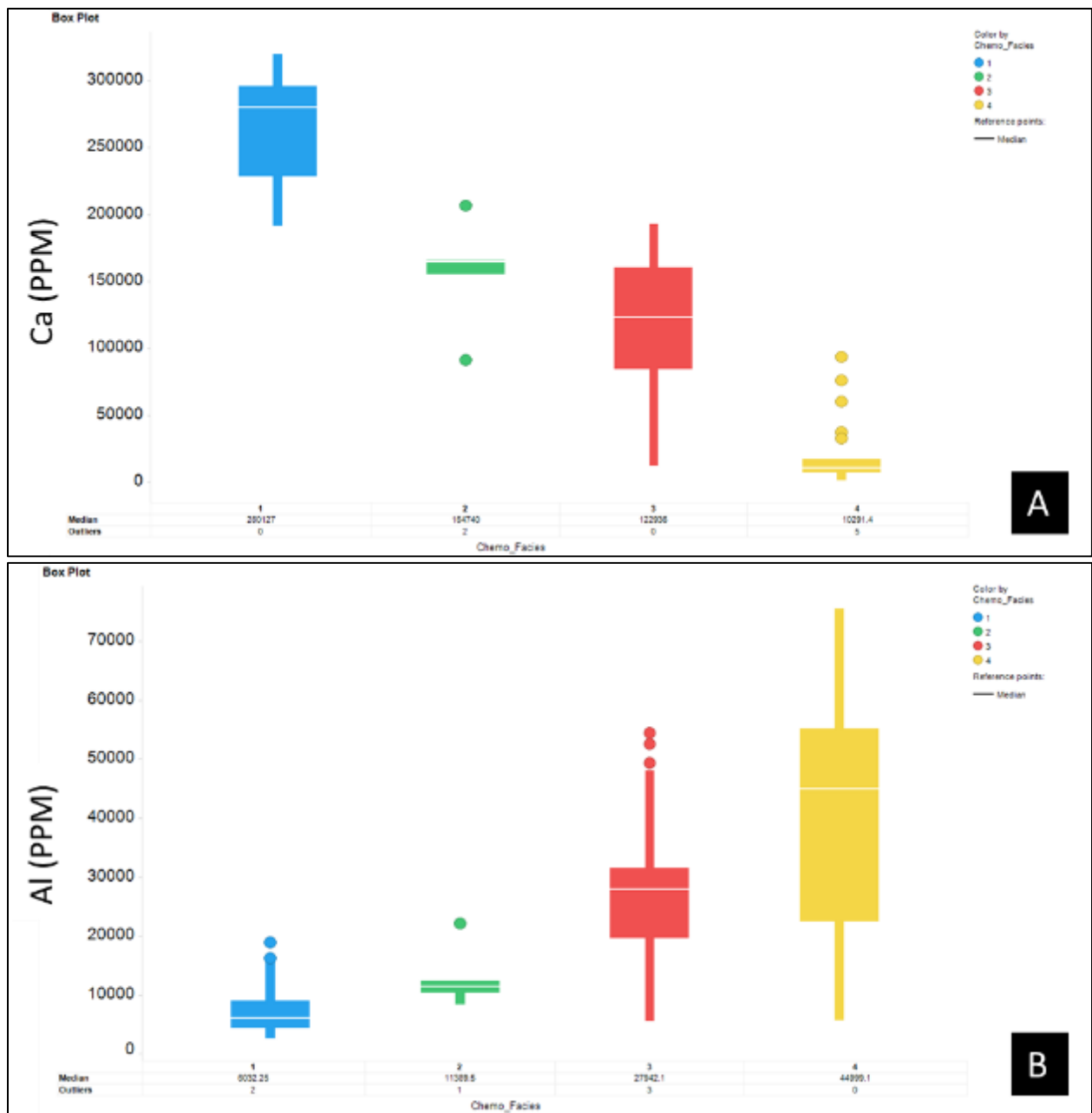
Figure 31— (A) depicts the relationship of each chemofacies to its abundance of a carbonate proxy calcium. (B) shows the relationship of each chemofacies to its abundance of a clay proxy aluminum. Chemofacies 3 and 4 are more clay rich and chemofacies 1 and 2 are more carbonate rich.
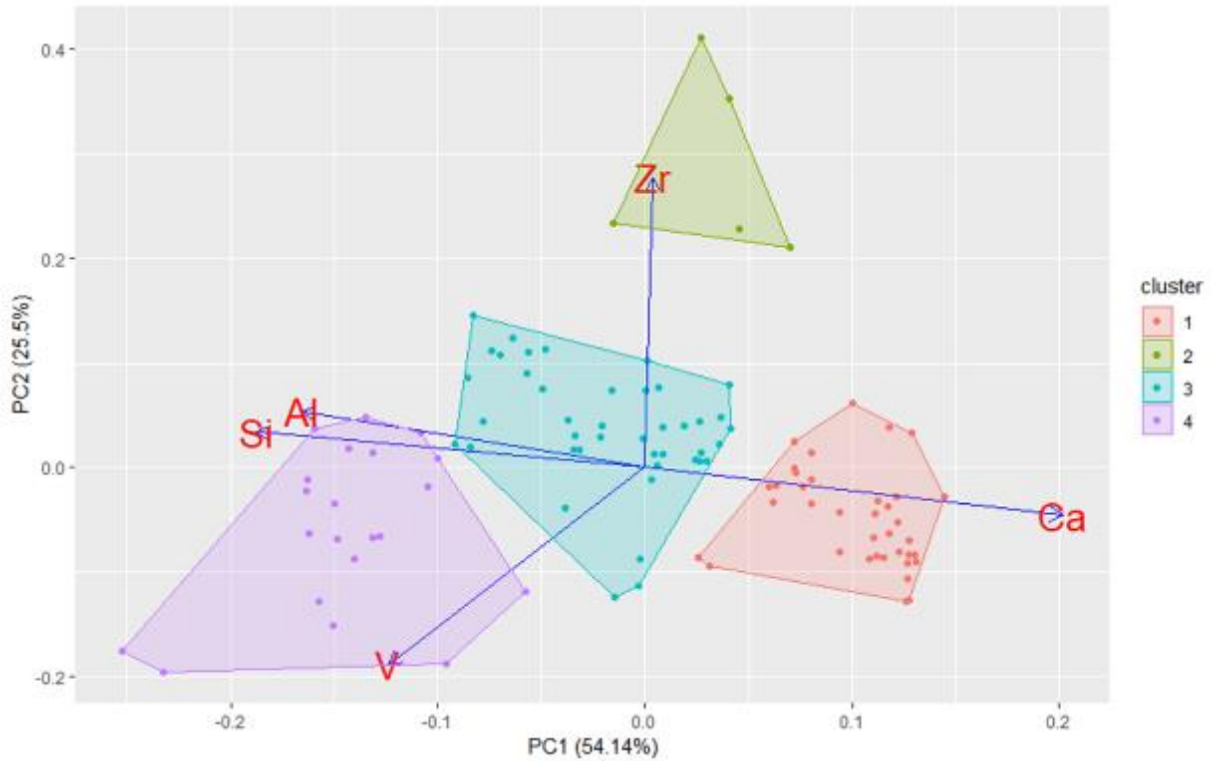
Figure 32— Principal component analysis with each cluster displayed and their related chemical proxy.
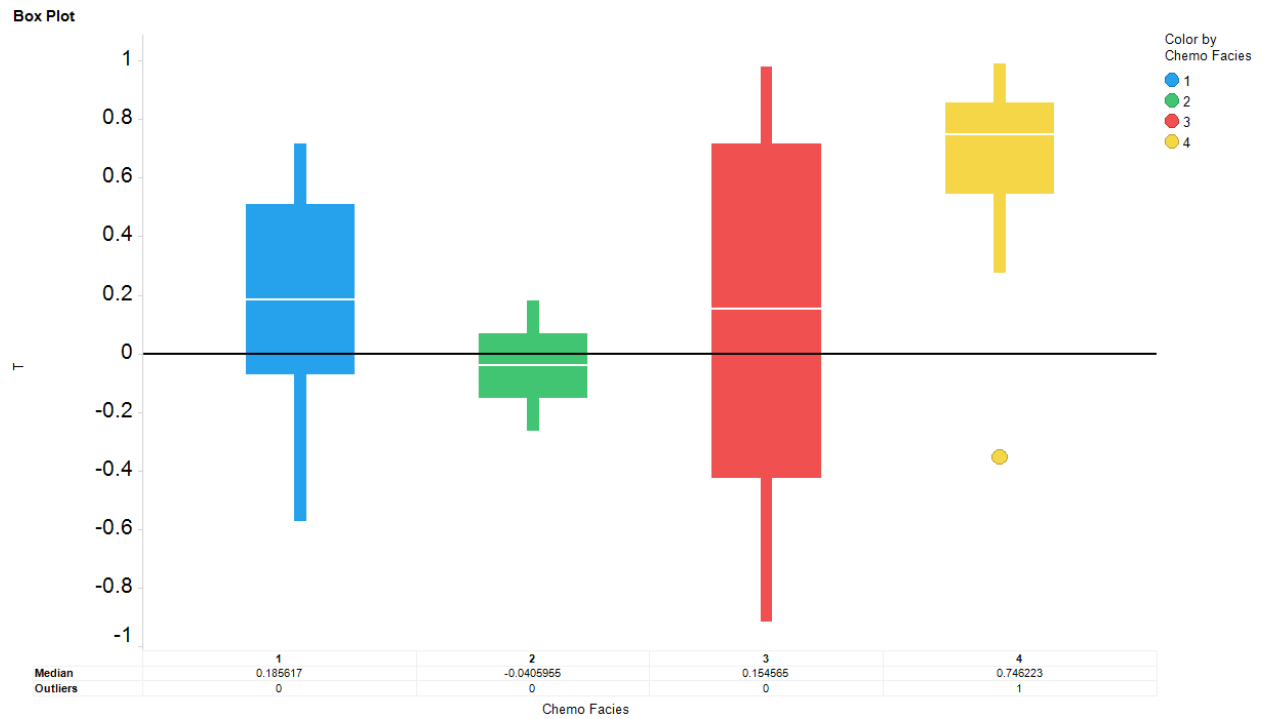
Figure 33— Chemofacies compared to shape factor (T). T>0 implies an oblate petrofabric, and T<0 implies a prolate petrofabric.
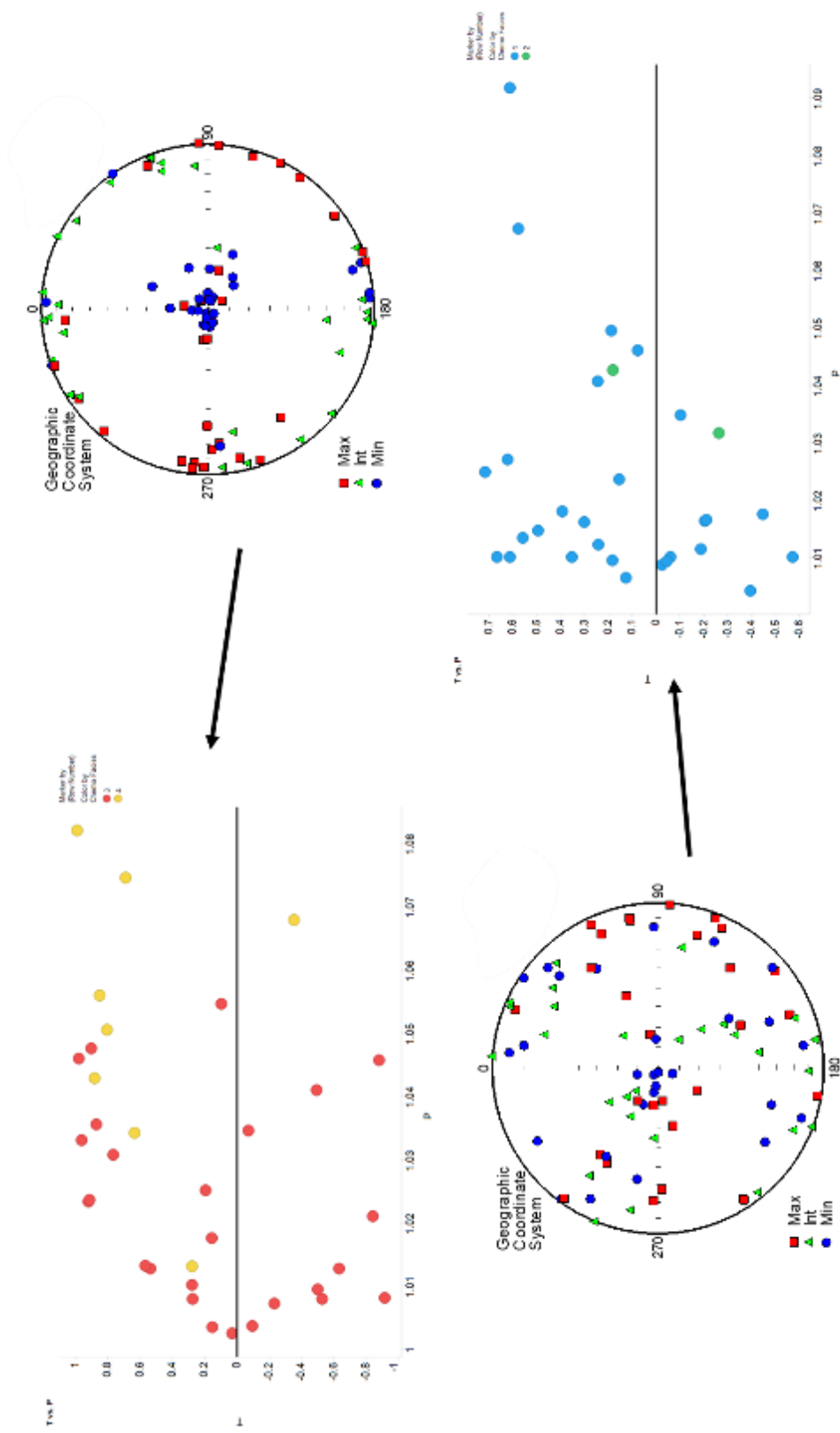
Figure 34— Distribution of prolate and oblate chemofacies in relation to shape factor (P).

	Argillaceous Siltstone	Argillaceous Spiculite	Bioturbated Siltstone	Calcitic Siltstone	Radiolarian Mudstone	Sandy Fossiliferous...	Silty Mudstone
Median	0.242373	-0.360592	0.537364	0.244363	0.181536	-0.0587	0.0917909
Outliers	0	0	1	1	1	0	0
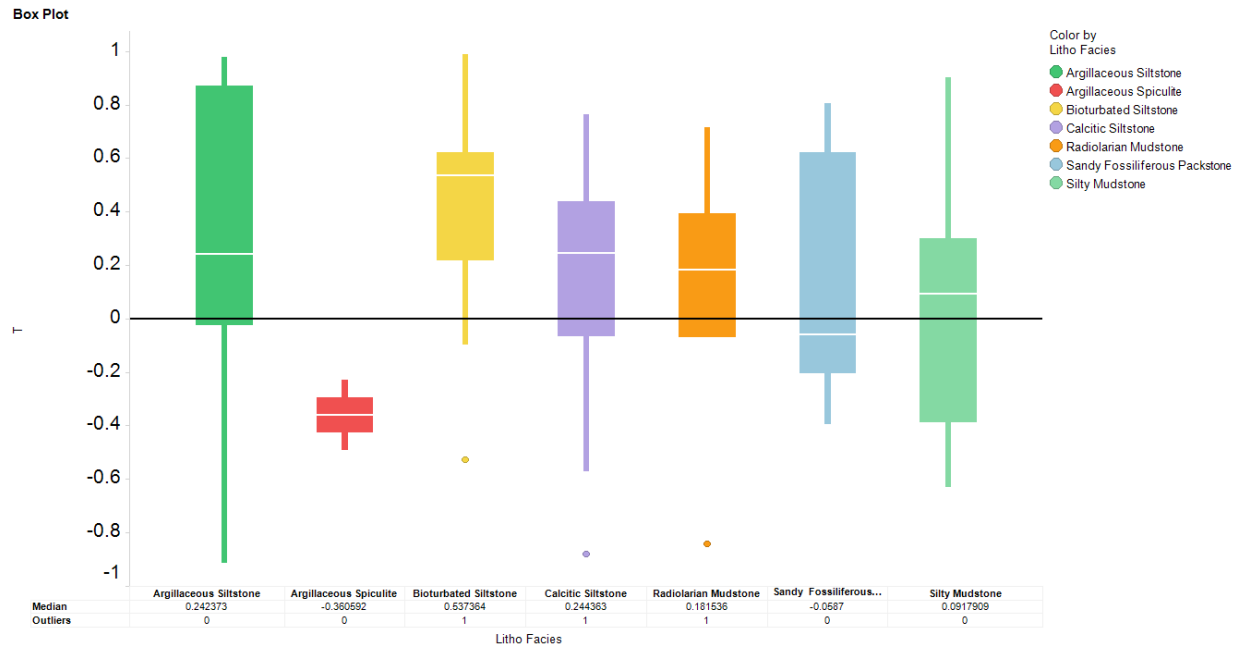
Figure 35— Lithofacies compared to shape factor (T). T>0 implies an oblate petrofabric, and T<0 implies a prolate petrofabric.
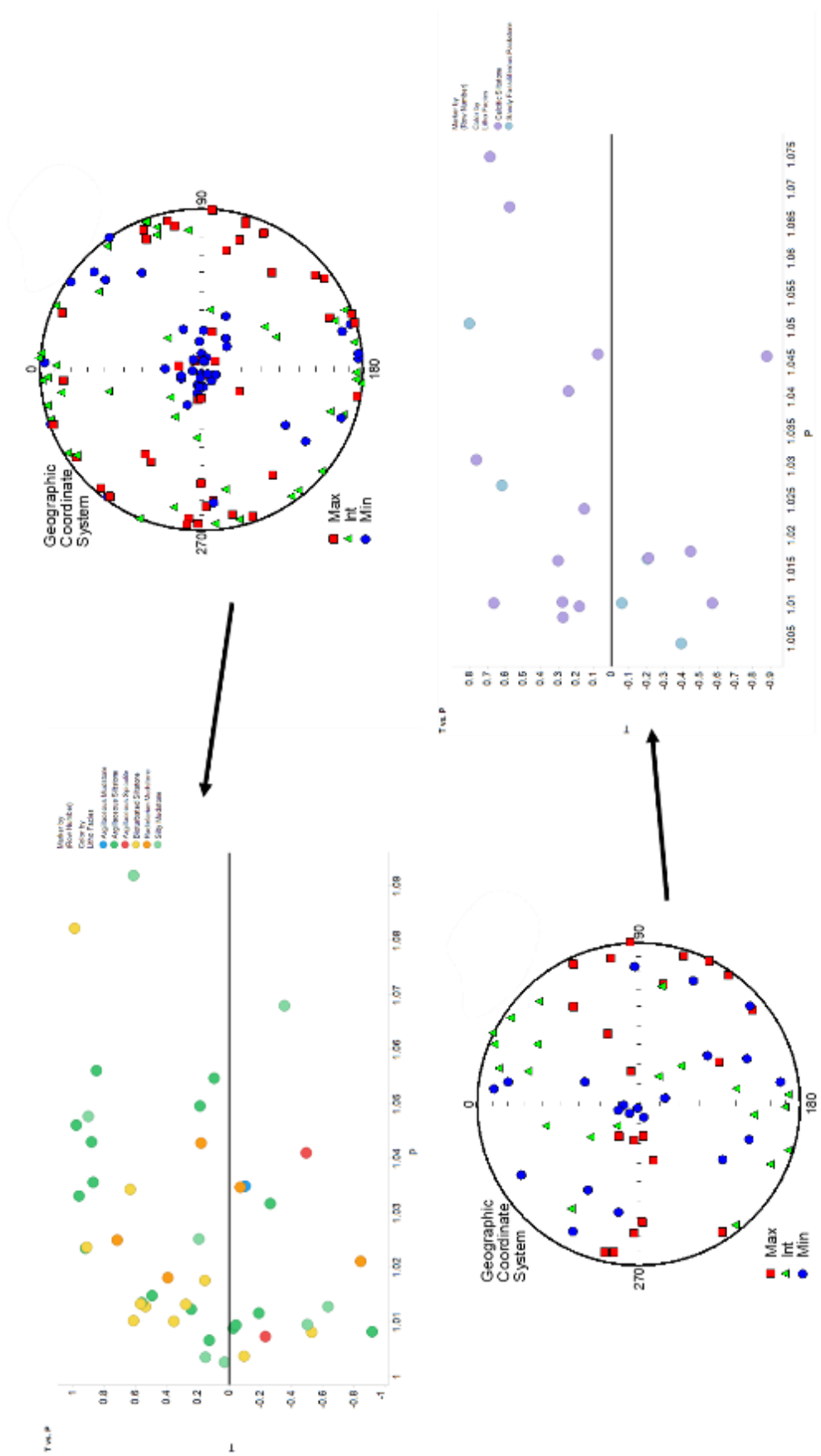
Figure 36— Distribution of prolate and oblate lithofacies in relation to shape factor (P).
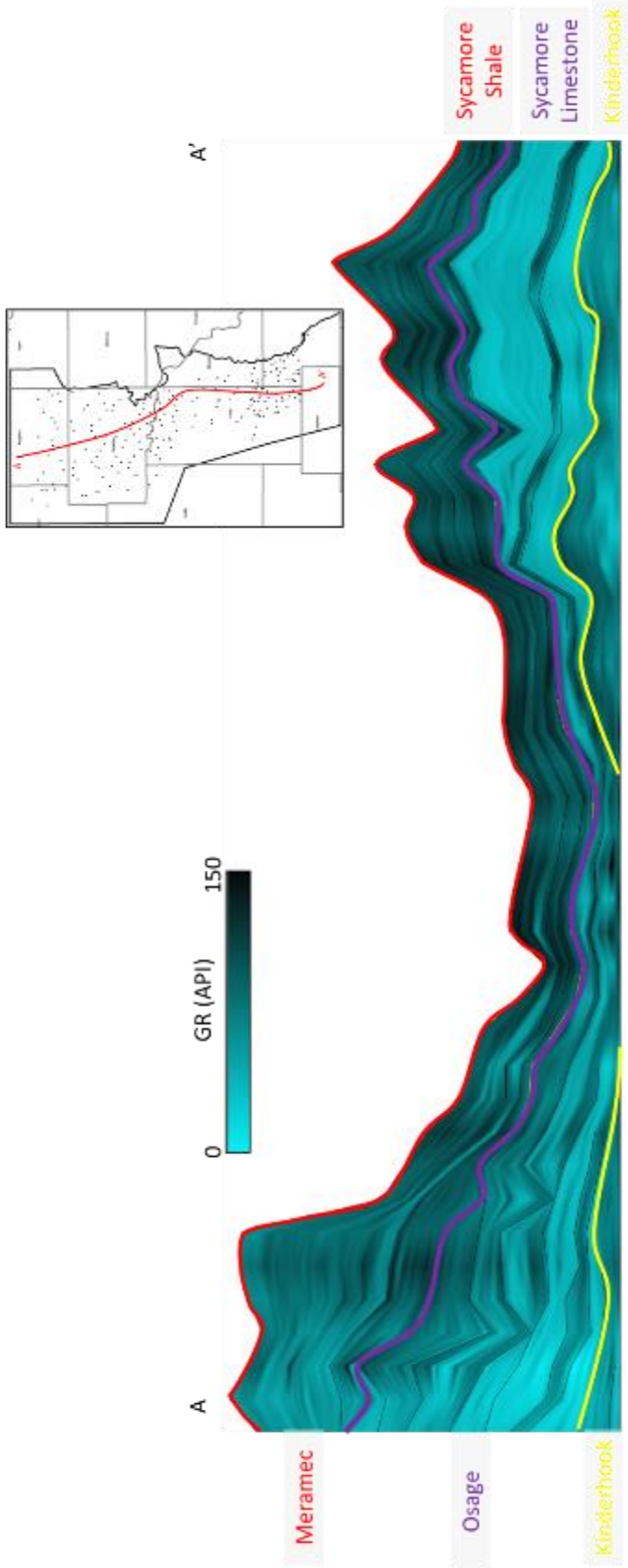
Figure 37—Cross section from the STACK to the SCOOP portion of the study area. The Meramec and Osage thin through the MERGE and increase in thickness in the SCOOP. The Meramec is correlative to the Sycamore Shale, and the Osage is correlative to the Sycamore Limestone.

70
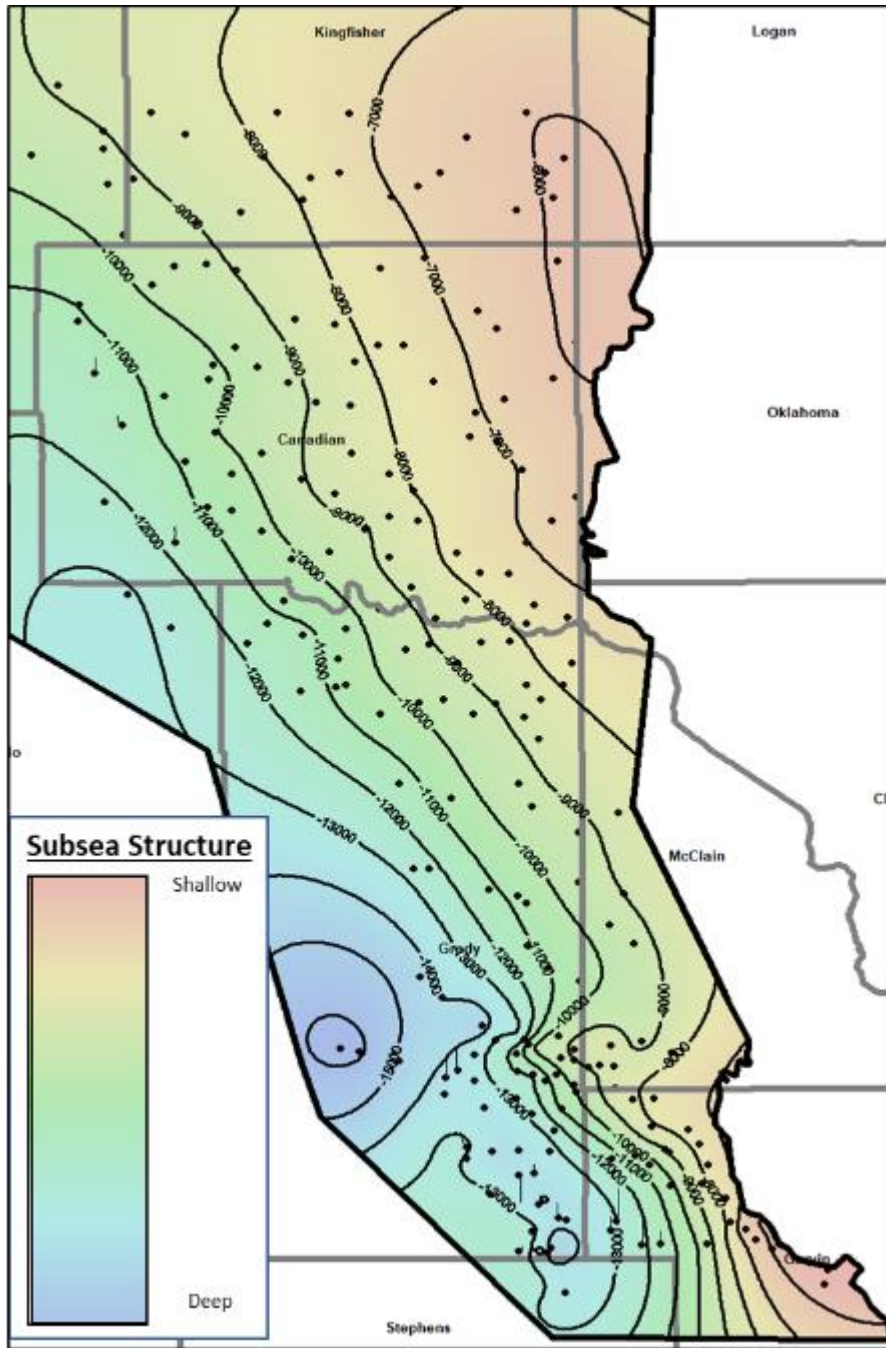
Figure 38— Woodford subsea structure map showing the structure deepening south and west into the Anadarko Basin.
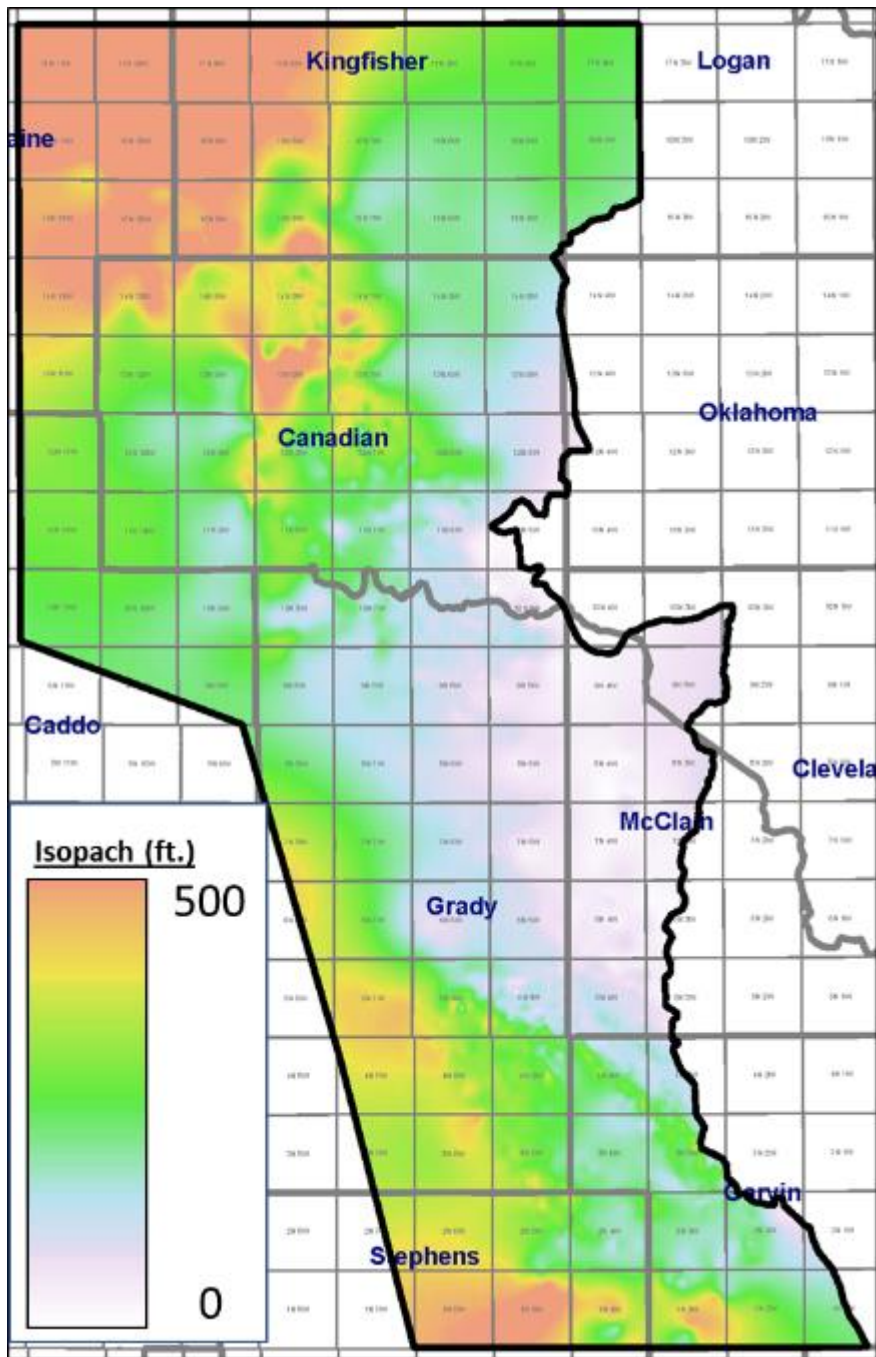
Figure 39— Osage isopach with thicknesses ranging from 0 to 500 feet [0 to 150 m].
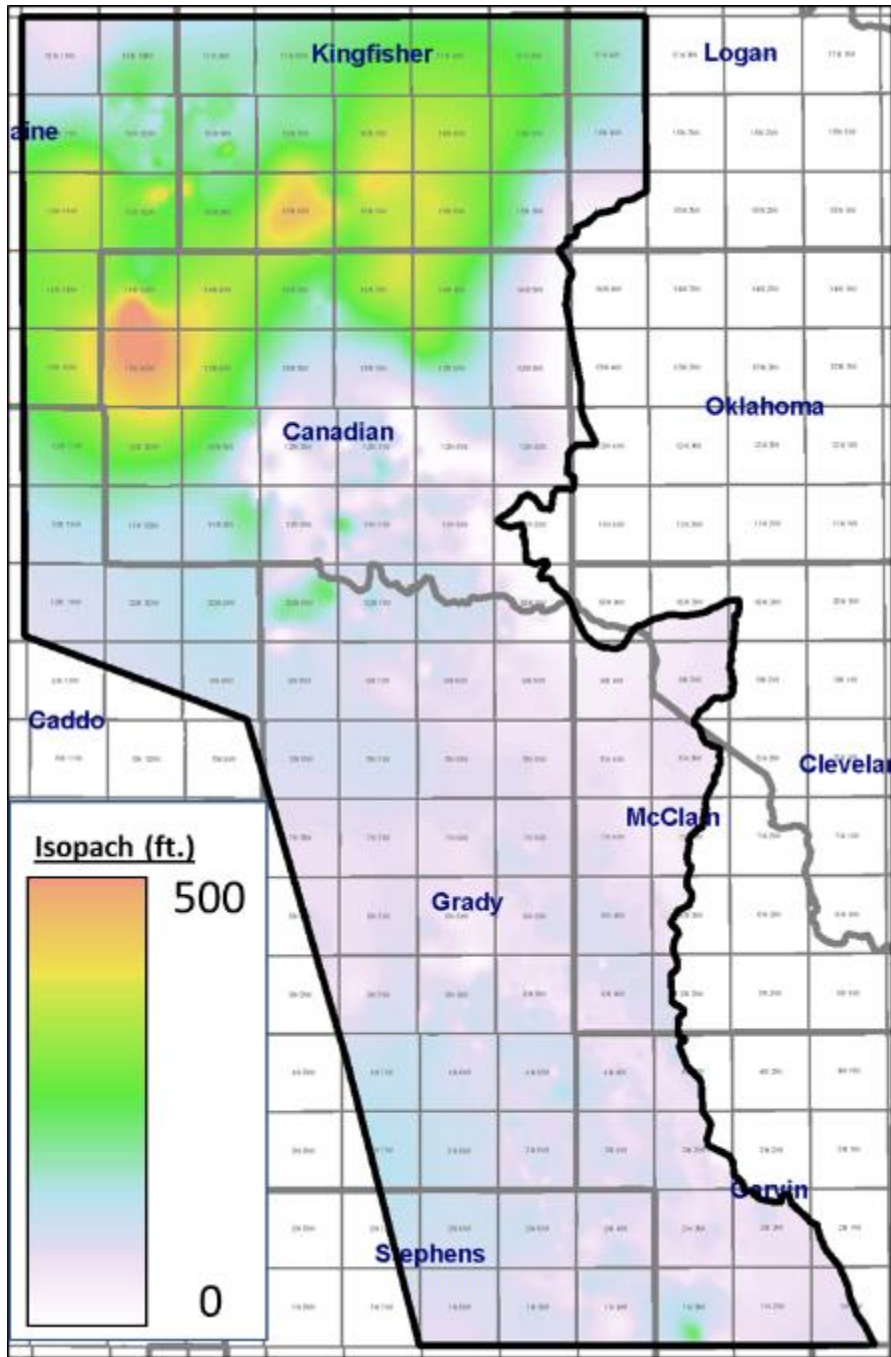
Figure 40— Meramec isopach with thicknesses ranging from 0 to 500 feet [0 to 150 m].

Tables

Mineral	Stain Result			Crystal Structure
	Alizarin Red S (ARS)	Potassium Ferricyanide (PF)	ARS & PF	
Calcite	Pink Orange	None	Pink Orange	Hexagonal
Ferroan Calcite	Pink Orange	Blue	Mauve, Purple Blue	
Dolomite	None	None	None	
Ferroan Dolomite	Pale Mauve	Blue Turqoise	Turqoise Green	
Siderite	None	None	None	
Magnesite	None	None	None	
Rhodochrosite	None	Pale Brown	Pale Brown	
Aragonite	Pink Orange	None	Pink Orange	Orthorhombic
Witherite	Red	None	Red	
Cerussite	Mauve	None	Mauve	

Table 1—Staining results from Alizarin Red and Potassium Ferricyanide. These stains were used in the identification of carbonate minerals and determining the extent of ferroan calcite zonation in the thin sections (Dickson, 1966; Precimat, 2018).

Proxy Element	Mineralogical/Environmental interpretation
Potassium (K)	Clay and feldspars
Aluminum (Al)	Clay and feldspars
Thorium (Th)	Clay
Silicon (Si)	Quartz
Calcium (Ca)	Carbonate
Strontium (Sr)	Carbonate
Molybdenum (Mo)	Anoxic bottom water
Vanadium (V)	Euxinic bottom water
Titanium (Ti)	Continental source
Zircon (Zr)	Continental source
Titanium/Niobium (Ti/Nb)	Mafic vs quartzofeldspathic source

Table 2—HHXRF elemental proxies and their associated mineralogical and environmental interpretation (Sageman & Lyons, 2003; Tribovillard et al., 2006; Turner et al., 2016, Duarte, 2018; Heij, 2018).

	Litho Facies	Al	Si	K	Ca	Ti	V	Th	Sr	Zr	Mo	Si/Al	Ti/Nb
Litho Facies	1.00												
Al	0.37	1.00											
Si	0.70	0.48	1.00										
K	0.46	0.92	0.54	1.00									
Ca	-0.68	-0.72	-0.89	-0.72	1.00								
Ti	0.17	0.86	0.41	0.81	-0.60	1.00							
V	0.59	0.12	0.46	0.22	-0.40	-0.08	1.00						
Th	0.49	0.86	0.55	0.95	-0.74	0.75	0.24	1.00					
Sr	-0.46	-0.66	-0.73	-0.63	0.83	-0.56	-0.35	-0.67	1.00				
Zr	-0.24	0.06	0.06	0.04	-0.06	0.42	-0.33	0.04	-0.11	1.00			
Mo	0.60	0.53	0.54	0.55	-0.69	0.33	0.63	0.61	-0.67	-0.18	1.00		
Si/Al	0.02	-0.60	0.05	-0.55	0.22	-0.61	0.36	-0.52	0.14	-0.15	-0.10	1.00	
Ti/Nb	0.10	0.75	0.25	0.61	-0.46	0.86	-0.08	0.50	-0.46	0.23	0.30	-0.54	1.00

Table 3—Correlation matrix for elements and ratios that are interpreted to be proxies for depositional conditions or mineral types. Green values are elements that have a correlation coefficient over .5 meaning a strong positive correlation. Red values are elements that have a correlation coefficient under -.5 implying the compared values have a strong negative correlation.

References

Asquith, G. B., Krygowski, D., Henderson, S., & Hurley, N. (2004). *Basic Well Log Analysis* (2nd ed.). Tulsa, OK: American Association of Petroleum Geologists.

Bathurst, R. G. C. (1966). Boring Algae, Micrite Envelopes and Lithification of Molluscan Biosparites. *Geological Journal*, *5*(1), 15-32. doi:10.1002/gj.3350050104

Blakey, R. C. (2013). Using Paleogeographic Maps to Portray Phanerozoic Geologic and Paleotectonic History of Western North America. *Search and Discovery*, *30267*, 1-61.

Bonjour, J. L., & Dabard, M. P. (1991). Ti/Nb Ratios of Clastic Terrigenous Sediments Used as an Indicator of Provenance. *Chemical Geology*, *91*(3), 257-267. doi:10.1016/0009-2541(91)90003-a

Boyd, D. T. (2008). Stratigraphic Guide to Oklahoma Oil and Gas Reservoirs. *Oklahoma Geological Survey: Special Publication*, *2008*(1). http://ogs.ou.edu/docs/specialpublications/SP2008-1P1.pdf

Culp, C. K. (1961). Stratigraphic Relations of the Sycamore Limestone (Mississippian) in Southern Oklahoma. *The Shale Shaker Digest, 3*(9), 446-457.

Dehcheshmehi, S. M. (2016). *Regional Diagenesis of Mississippian Strata of the Southern Mid-Continent, USA* (Doctoral dissertation, Oklahoma State University). Retrieved from https://shareok.org/bitstream/handle/11244/54573/MohammadiDehcheshmehi_okstate_0664D_14872.pdf

Dickson, J. A. D. (1966). Carbonate Identification and Genesis as Revealed by Staining. *Journal of Sedimentary Research*, *36*(2), 491-505. doi:10.1306/74d714f6-2b21-11d7-8648000102c1865d

Domeier, M., & Torsvik, T. H. (2014). Plate Tectonics in the Late Paleozoic. *Geoscience Frontiers, 5*, 303-350. https://doi.org/10.1016/j.gsf.2014.01.002

Drummond, K. (2018). *Regional Stratigraphy and Proximal to Distal Variation of Lithology and Porosity Within a Mixed Carbonate-Siliciclastic System, Meramec And Osage Series (Mississippian), Central Oklahoma* (Master's thesis, University of Oklahoma). Retrieved from https://shareok.org/handle/11244/301995

Duarte, D. (2018). *Rock Characterization and Stratigraphy of the Mississippian Strata, Meramec / Sycamore. Merge Play, Central Oklahoma* (Master's thesis, University of Oklahoma). Retrieved from https://shareok.org/handle/11244/316322

Dubey, A. (2014). *Understanding an Orogenic Belt: Structural Evolution of the Himalaya.* Switzerland: Springer International Publishing. 17-32. doi:10.1007/978-3-319-05588-6

Elmore, R. D., Haynes, J., Farzaneh, S., & Anzaldua, S. (2015). Integrated Diagenetic and Paleomagnetic Study of the Mississippian Limestone, North Central Oklahoma. *Search and Discovery, 51163*, 7-27.

Elmore, R. D., Haynes, J., Farzaneh, S., & Anzaldua, S. (2017). Integrated paleomagnetic and diagenetic study of the Mississippian Limestone, North Central Oklahoma. *AAPG Memoir, 116,* doi:10.1306/13632156M11667.

Folk, R. L. (2005). Nanobacteria and the Formation of Framboidal Pyrite: Textural Evidence. *Journal of Earth System Science, 114*(3), 369-374. doi:10.1007/bf02702955

Franklin, K. (1997). *The Depositional History of the Sycamore Limestone* (Master's thesis, Oklahoma State University). Retrieved from https://shareok.org/handle/11244/10888

Garner, D. L., & Turcotte, D. L. (1984). The Thermal and Mechanical Evolution of the Anadarko Basin. *Tectonophysics, 107*(1-2), 1-24. doi:10.1016/0040-1951(84)90026-x

Goldstein, R., & King, B. (2015). Impact of Hydrothermal Fluid Flow on Conventional and

      Unconventional Carbonate-Rich Reservoirs, Midcontinent USA. *Search and Discovery,*

      51085, 1-24.

Golonka, J., Ross, M. I., & Scotese, C. R. (1994). Phanerozoic Paleogeographic and

      Paleoclimatic Modeling Maps, Pangea: Global Environments and Resources. *Canadian*

      Society of Petroleum Geologists Memoir, 17, 1-47.

Gutschick, R. C., & Sandberg, C. A. (1983). Mississippian Continental Margins of the

      Conterminous United States. *Society of Economic Paleontologists and Mineralogists:*

      Special Publication, 33, 79-96. doi:10.2110/pec.83.06.0079

Ham, W. E., & Wilson, J. L. (1967). Paleozoic Epeirogeny and Orogeny in the Central United

      States. *American Journal of Science, 265*(5), 332-407. doi:10.2475/ajs.265.5.332

Ham, W. E., Denison, R. E., & Merritt, C. A. (1964). Basement Rocks and Structural Evolution

      of Southern Oklahoma. *Oklahoma Geological Survey Bulletin, 95*, 1-302.

      doi:10.1306/bc743c77-16be-11d7-8645000102c1865d

Hardwick, J. (2018). *Reservoir Quality Evaluation of the Meramec and Upper Osage Units in*

      the Anadarko Basin (Master's thesis, University of Oklahoma). Retrieved from

      https://shareok.org/handle/11244/316227

Hartigan, J. A. & Wong, M. A. (1979). Algorithm AS 136: A K-Means Clustering Algorithm.

      Journal of the Royal Statistical Society. Series C, *28*(1), 100-108.

      https://doi.org/10.2307/2346830

Heij, G. (2018). *Magnetic Fabrics and Paleomagnetism of North American Mudrocks: Relics of*

      Complex Burial Histories (Doctoral dissertation, University of Oklahoma). Retrieved

      from https://shareok.org/handle/11244/316294

Hoffman, P., Dewey, J. F., & Burke, K. (1974). Aulacogens and their Genetic Relation to
Geosynclines, with a Proterozoic Example from Great Slave Lake, Canada. *Modern and Ancient Geosynclinal Sedimentation*, 38-55. doi:10.2110/pec.74.19.0038

Hrouda, F. (2002). Low-field Variation of Magnetic Susceptibility and its Effect on the
Anisotropy of Magnetic Susceptibility of Rocks. *Geophysical Journal International, 150*(3), 715-723. https://doi.org/10.1046/j.1365-246X.2002.01731.x

Hrouda, F., Chlupáčová, M., & Mrázová, Š. (2006). Low-field Variation of Magnetic
Susceptibility as a Tool for Magnetic Mineralogy of Rocks. *Physics of the Earth and Planetary Interiors, 154*(3-4), 323-336. http://doi.org/10.1016/j.pepi.2005.09.013

Jelinek, V. (1981). Characterization of the Magnetic Fabric of Rocks. *Tectonophysics, 79*(3-4),
63-67. doi: 10.1016/0040-1951(81)90110-4

Johnson, K. & Cardott, B. (1992). Geologic Framework and Hydrocarbon Source Rocks of
Oklahoma. *Oklahoma Geological Survey Circular, 93*, 21-37.

Kanungo, T., Mount, D. M., Netanyahu, N. S., Piatko, C. D., Silverman, R., & Wu, A. Y. (2002).
An Efficient K-Means Clustering Algorithm: Analysis and Implementation. *IEEE Transactions on Pattern Analysis and Machine Intelligence*, *24*(7), 881-892.

Knaust, D. (2017). *Atlas of Trace Fossils in Well Core Appearance, Taxonomy and
Interpretation.* Switzerland: Springer International Publishing. 1-209, doi:10.1007/978-3-319-49837-9.

Leavitt, A. (2018). Depositional Systems of the STACK and SCOOP Mississippian Units:
Regional Understanding from Logs and Core. *The STACK Play Workshop, Oklahoma Geological Survey.*

Manger, W. L. (2014). Tripolitic Chert Development in the Mississippian Lime: New Insights from SEM. *Search and Discovery,50957*, 1-39.

Mazzullo, S. J., Wilhite, B. W., & Woolsey, I. W. (2009). Petroleum Reservoirs within a Spiculite-Dominated Depositional Sequence: Cowley Formation (Mississippian: Lower Carboniferous), South-Central Kansas. *AAPG Bulletin, 93*(12), 1649-1689. doi:10.1306/06220909026

Miller, J. (2018). *Regional Stratigraphy and Organic Richness of the Mississippian Meramec and Associated Strata, Anadarko Basin, Central Oklahoma* (Master's thesis, University of Oklahoma). Retrieved from https://shareok.org/handle/11244/299846

Mueller, P. A., Heatherington, A. L., Foster, D. A., Thomas, W. A., & Wooden, J. L. (2014). The Suwannee Suture: Significance for Gondwana-Laurentia Terrane Transfer and Formation of Pangaea. *Gondwana Research, 26*(1), 365-373. doi:10.1016/j.gr.2013.06.018

Northcutt, R. A. & Campbell, J. A. (1995). Geologic Provinces of Oklahoma. *Basement Tectonics, 12*, 29-37.

Parés, J. M. (2015). Sixty Years of Anisotropy of Magnetic Susceptibility in Deformed Sedimentary Rocks. *Frontiers in Earth Science, 3*, 1-17. doi:10.3389/feart.2015.00004

Patruno, S., Hampson, G. J., & Jackson, C. A. (2015). Quantitative Characterization of Deltaic and Subaqueous Clinoforms. *Earth-Science Reviews, 142*, 79-119. doi:10.1016/j.earscirev.2015.01.004

Perry, W. J. (1989). Tectonic Evolution of the Anadarko Basin Region, Oklahoma. *U.S. Geological Survey Bulletin, 1866-A*, 1-28. doi:10.3133/b1866a

Precimat. (2018). *Thin Section Manufacturing & Petrographic Analysis*. Retrieved from www.precimat.com/services/petrographic-manufacturing/thin-sections/

Price, B. (2014). *High Resolution Sequence Stratigraphic Architecture and Reservoir Characterization of the Mississippian Bentonville Formation, Northwestern Arkansas* (Master's thesis, Oklahoma State University). Retrieved from https://shareok.org/handle/11244/25705

Price, B., Haustveit, K., & Lamb, A. (2017). Influence of Stratigraphy on Barriers to Fracture Growth and Completion Optimization in the Meramec Stack Play, Anadarko Basin, Oklahoma. *Unconventional Resources Technology Conference*, 2697585, 1-8. doi: 10.15530/URTEC-2017-2697585

Read, J. (1985). Carbonate Platform Facies Models. *AAPG Bulletin, 69*, 1-21. doi:10.1306/ad461b79-16f7-11d7-8645000102c1865d

Read, J., Kerans, C., Weber, J. L., Sarg, J. F., & Wright, F. M. (1995). Overview of Carbonate Platform Sequences, Cycle Stratigraphy and Reservoirs in Greenhouse and Ice-House Worlds, Milankovitch Sea-Level Changes. *SEPM Short Couse, 35*, 1-102. doi:10.2110/scn.95.35.0001.

Ries, J. B. (2010). Geological and Experimental Evidence for Secular Variation in Seawater Mg/Ca (Calcite-Aragonite Seas) and its Effects on Marine Biological Calcification. *Biogeosciences, 7*(9), 2795-2849. doi:10.5194/bg-7-2795-2010

Roberts, J. & Elmore, D. (2017). A Diagenetic Study of the Woodford Shale in the Southeastern Anadarko Basin, Oklahoma, USA: Evidence for Hydrothermal Alteration in Mineralized Fractures. *Interpretation, 6*(1), 1-40. https://doi.org/10.1190/INT-2017-0071.1

Rogers, S. M. (2001). Deposition and Diagenesis of Mississippian Chat Reservoirs, North-Central Oklahoma. *AAPG Bulletin, 85*(1), 115-129. doi:10.1306/8626c771-173b-11d7-8645000102c1865d

Rowe, H., Hughes, N., & Robinson, K. (2012). The Quantification and Application of Handheld Energy-Dispersive X-Ray Fluorescence (ED-XRF) in Mudrock Chemostratigraphy and Geochemistry. *Chemical Geology, 324-325*, 122-131. doi:10.1016/j.chemgeo.2011.12.023

Sageman, B. B., & Lyons, T. W. (2003) Geochemistry of Fine-Grained Sediments and Sedimentary Rock. *Treatise on Geochemistry, 7*, 115-158. doi:10.1016/b0-08-043751-6/07157-7.

Schlumberger. (1991). *Log Interpretation Principles/Applications*. New York, NY: Schlumberger Educational Services.

Schmidt, V., Hirt, A. M., Rosselli, P., & Martín-Hernández, F. (2007). Separation of Diamagnetic and Paramagnetic Anisotropy by High-Field, Low-Temperature Torque Measurements. *Geophysical Journal International*, *168*(1), 40-47. https://doi.org/10.1111/j.1365-246X.2006.03202.x

Schwartzapfel, J. A. & Holdsworth, B. K. (1996). Upper Devonian and Mississippian Radiolarian Zonation and Biostratigraphy of the Woodford, Sycamore, Caney and Goddard Formations, Oklahoma. *Cushman Foundation for Foraminiferal Research Special Publication, 33*, p. 275.

Taff, J. A. (1903). Tishomingo Folio, Indian Territory. *Tisholningo Folio, 98*, 1-5. doi:10.3133/gf98

Tarling, D. H. & Hrouda, F. (1993). The Magnetic Anisotropy of Rocks. *Chapman & Hall*, 1-217.

Thyberg, B., Jahren, J., Winje, T., Bjorlykke, K., Faleide, J. I., & Marcussen, O. (2010). Quartz Cementation in Late Cretaceous Mudstones, Northern North Sea: Changes in Rock

Properties Due to Dissolution of Smectite and Precipitation of Micro-Quartz Crystals. *Marine and Petroleum Geology, 27*(8), 1752-1764. doi:10.1016/j.marpetgeo.2009.07.005

Tribovillard, N., Algeo, T. J., Lyons, T., & Ribolleua, A. (2006). Trace Metals as Paleoredox and Paleoproductivity Proxies: An Update. *Chemical Geology, 232*(1-2), 12-32. doi:10.1016/j.chemgeo.2006.02.012.

Turner, B. W., Treanton, J., & Slatt, R. (2016). The Use of Chemostratigraphy to Refine Ambiguous Sequence Stratigraphic Correlations in Marine Shales: An Example from the Woodford Shale, Oklahoma. *Journal of the Geological Society, 173*(5), 1-16. doi:10.2118/178574-ms.

Witzke, B. J. (1990). Paleoclimatic Constraints for Paleozoic Paleolatitudes of Laurentia and Euramerica. *Geological Society, London, Memoirs, 12*(1), 57-73. doi: 10.1144/gsl.mem.1990.012.01.05.